NASA

Technical Memorandum 85086

SURVEY OF LOW ENERGY PLASMA ELECTRONS IN SATURN'S MAGNETOSPHERE: VOYAGERS 1 AND 2

E. C. Sittler, Jr.
K. W. Ogilvie
J. D. Scudder

SEPTEMBER 1983

National Aeronautics and
Space Administration

Goddard Space Flight Center
Greenbelt, Maryland 20771

SURVEY OF LOW ENERGY PLASMA ELECTRONS IN SATURN'S MAGNETOSPHERE: VOYAGERS 1 AND 2

E. C. Sittler, Jr.
K. W. Ogilvie
J. D. Scudder
NASA/Goddard Space Flight Center
Laboratory for Extraterrestrial Physics
Greenbelt, MD 20771

ABSTRACT

This paper is a survey of the low energy plasma electron environment within Saturn's magnetosphere made by the Plasma Science Experiment (PLS) during the Voyager encounters with Saturn. Over the full energy range of the PLS instrument (10 eV to 6 keV) the electron distribution functions are clearly non-Maxwellian in character; they are composed of a cold (thermal) component with Maxwellian shape and a hot (suprathermal) non-Maxwellian component.

A large scale positive radial gradient in electron temperature is observed, increasing from less than 1 eV in the inner magnetosphere to as high as 800 eV in the outer magnetosphere. This increase in electron temperature explains the observed order of magnitude increase in plasma sheet thickness with increasing radial distance from Saturn. Scale heights of the cold heavy ion plasma can be as small as 0.2 R_S in the inner magnetosphere and as much as 3 R_S in the outer magnetosphere. Many of the observed density variations can be attributed to changes in density scale height without a change in plasma flux tube content.

Three fundamentally different plasma regimes have been identified from the measurements: (1) the hot outer magnetosphere, (2) the extended plasma sheet, and (3) the inner plasma torus. The hot outer magnetosphere is a region within which the suprathermal electrons are the dominant contributors to the electron pressure, and at times to the electron density. Near the noon meridian, the electrons display a highly time dependent behavior with order of magnitude changes in density and temperature, which can occur in less than 96 seconds. Sudden density enhancements of cold plasma occur, which are thought to be either "plumes" associated with Titan (Eviatar et al., 1982) or plasma "blobs", Goertz (1983). The extended plasma sheet, with mean inner and outer boundaries of 7 and 15 R_S respectively, has enhanced levels of cold plasma relative to that in the hot outer magnetosphere, although the suprathermals continue to dominate the electron pressure. Plasma with energy less than 6 keV from this region is an important contributor to the ring current, and a significant current system is probably present between 6 and 8 R_S. The

inner plasma torus is a region of reduced electron temperature (as low as 1 eV), enhanced equatorial densities (as high as 100/cm^3) and reduced scale height (as small as 0.2 R_s). Localized reductions in electron temperature are observed near the L shells of Tethys, Dione, and possibly Rhea. The suprathermal electrons are observed to be severely depleted within the inner plasma torus, relative to that in the extended plasma sheet and hot outer magnetosphere. The energy dependence of the depletions indicate an interaction with dust or plasma waves at times; interactions with neutral gas or plasma ions may also contribute to the depletions. The data also indicate an association between the appearance of suprathermal electrons and the observed emission of whistler mode waves reported by Gurnett et al. (1981).

1. Introduction

Preliminary analysis of ion and electron plasma measurements made during the Voyager 1 and 2 encounters with Saturn in November 1980 and August 1981, respectively, were presented by Bridge et al. (1981, 1982). Additional papers resulting from the analysis of this data set are the publications by Sittler et al. (1981), Hartle et al. (1982), Eviatar et al. (1982, 1983), Lazarus et al. (1983) and Goertz (1983). This paper presents new results obtained from further analysis of the electron plasma measurements at Saturn. Results from the ion analysis are given in an accompanying paper by Lazarus and McNutt (1983). In many respects the results presented in these papers are complementary, and should be considered together to form a coordinated picture of Saturn's plasma environment.

Essential trajectory information is presented in section 2, followed by a brief description of instrument operation in section 3. A detailed description of the analysis is given in a separate publication by Sittler (1983). Section 4 surveys the electron observations and their implications within Saturn's magnetosphere and defines the three principal sub-regimes: 1) the hot outer magnetosphere, 2) the extended plasma sheet, and 3) the inner plasma torus. Sections 5, 6 and 7 give a more detailed discussion of the observations within the three sub-regimes defined in section 4. In section 7 the primary emphasis of the discussion is on the observed depletion of suprathermal electrons and low electron temperatures observed within the inner plasma torus. In section 8 we discuss the apparent relationship within the inner magnetosphere between the presence of suprathermal electrons and whistler mode emissions reported by Gurnett et al. (1981). Section 9 discusses the relationship between the plasma observations and Saturn's ring current as modeled by the magnetometer team (Connerney et al., 1981). Lastly, section 10 consists of a summary and interpretation of the observations.

2. Pioneer 11, Voyager 1 and 2 Trajectories

Equatorial and meridional views of the trajectories of the Pioneer 11 and Voyager 1 and 2 spacecraft are displayed in Figure 1 in a Saturn centered coordinate system.

As shown in Figure 1a all three spacecraft approached Saturn near the noon meridian. Both Voyager 2 and Pioneer 11 left the magnetosphere of Saturn near the dawn meridian; Voyager 1 exited further down the tail at a local time ~0330. To show the characteristic dimensions of Saturn's magnetosphere we have superimposed "average" modeled bow shock and magnetopause boundaries upon Figure 1a, as described in Bridge et al. (1982), and indicated the observed bow shock (S) and magnetopause crossings (M) for each spacecraft as reported in Bridge et al. (1981, 1982) for Voyager 1 and 2 and Wolfe et al. (1980) for Pioneer 11.

The average position of the sub-solar point is ~21 R_S (intermediate in relative size between Earth ~10 R_E and Jupiter ~50 R_J), just outside the orbit of Titan; this position can vary considerably depending on external solar wind conditions; thus Titan is not always inside the magnetosphere of Saturn. Voyager 1 left the magnetosphere at a radial distance of 43 R_S from Saturn which is somewhat closer than average conditions would dictate. By contrast, Voyager 2 and Pioneer 11 observed magnetopause and bow shock crossings well outside their average positions. This wide variability in position of the boundary crossings is indicative of the great variability of the external solar wind ram pressure at these large radial distances (Lazarus and Gazis, 1983, Burlaga et al., 1983, Burlaga, 1983). In the case of Voyager 2, as noted in Bridge et al. (1982), the observed inflation of the magnetosphere during the outbound portion of the trajectory may have been a result of Saturn being within Jupiter's magnetotail. Recent publications by Kurth et al. (1981a), Scarf et al. (1981), Lepping et al. (1982, 1983), Kurth et al. (1982) and Desch (1983) using plasma, magnetic field and plasma wave data obtained during the cruise phase of the Voyager mission between Jupiter and Saturn encounters, present convincing evidence that Jupiter's tail probably extends beyond the orbit of Saturn and that Saturn could have been within Jupiter's tail at the time of the Voyager 2 encounter.

Figure 1b shows that the Pioneer 11 spacecraft was confined near the equatorial plane throughout its encounter with Saturn. Voyager 1 approached Saturn at low latitudes and left the magnetosphere at large northerly latitudes. Voyager 2 was at high latitudes for most of its encounter except near closest approach when crossing the ring plane.

For reference purposes we have superimposed dipole field lines in Figure 1b. There are corrections to Saturn's dipole field, as evolving model calculations by Connerney et al. (1981, 1982) suggest the presence of quadrupole and octupole terms in the internal field and a ring current between L=8.5 and 15.5; these corrections become important outside L=8, where the ring current produces an inflation of the dipole field lines. The lack of tilt in most magnetic field models makes the spin equator nearly congruent with the magnetic equator. This has the unfortunate consequence that each spacecraft does not make as many crossings of Saturn's plasma sheet during an encounter as was the case during the Jupiter encounters. This symmetry, however, produces a simplification in our interpretation of the plasma data, as it makes the centrifugal and magnetic equatorial planes nearly coincident. Under this condition, the plasma, regardless of its thermal characteristics, will have mirror symmetry about the equatorial plane. As noted in Smith et al. (1980), the corotational electric field can dominate the convective electric field due to the solar wind out to radial distances in excess of 21 R_S, the average radial position of the noon time magnetopause boundary. In first approximation, one expects Saturn's magnetosphere to be azimuthally symmetric inside L=15; the magnetic field data reported by Smith et al. (1980) and Ness et al. (1981, 1982) support this expectation. Finally, using the above approximations of dipole field, mirror symmetry, azimuthal symmetry, and making the additional assumption of "steady-state" one can increase the coverage of the spatial distribution of the plasma in L, Z space by combining the plasma data from all three encounters. In this way, Bridge et al. (1982) were able to construct a fairly extensive description of the plasma morphology.

3. Instrumentation

The Plasma Science Instrument on Voyager makes both positive ion and electron measurements covering the energy per charge range from 10 eV to 5950 eV. A detailed description of the instrument is given in Bridge et al. (1977). Briefly, the instrument is composed of four potential modulated Faraday cups denoted by the letters A, B, C and D. The three main sensors A, B and C make only positive ion measurements and, except for rare brief spacecraft maneuvers, are always pointed nearly along the spacecraft-Sun line. The side sensor or D cup makes both positive ion and electron measurements and is normally oriented nearly at right angles to the solar direction. The angular response of the side sensor is cylindrically symmetric about its look direction, and provides a field of view with conical half angle $\sim 30^{\circ}$(FWHM) about its normal. The D sensor makes differential contiguous measurements of the electron distribution function along the sensor normal. It was aligned to respond to the azimuthal flow for both Voyager 1 and 2 during their inbound approaches to Saturn. Outbound, only Voyager 1 was oriented so as to provide some sensitivity to the azimuthal ion flow. Because the electron thermal speeds are much larger than flow speeds of the plasma, electron measurements are not very sensitive to sensor orientation, unless there are large pressure anisotropies. Since the instrument angular field of view is fairly broad, uncertainties due to pressure anisotropies are not expected to have an important effect upon our analysis.

The side sensor completes a measurement cycle in 96 seconds during which it passes through the mode sequence M, E1, L and E2. M and L are the high and low resolution positive ion modes, respectively, while E1 and E2 (see Figure 4 in Sittler, 1983) are the low and high energy electron modes, respectively. The energy range for E1 is 10 eV to 140 eV while for E2 it is 140 eV to 5950 eV. Each electron mode is composed of 16 continguously spaced energy channels; for the E2 mode only the upper 12 channels are used. The channels for E1 are nearly equally spaced in energy ($.099 < \Delta E/E < .37$), while for E2 they are more logarithmically spaced ($\Delta E/E = .29$). The sampling time for both energy modes is 3.84 seconds and E1 and E2 modes are separated in time by 45 seconds. This large time gap between low and

high electron energy measurements can result in discontinuous changes in the composite energy spectrum across the 140 eV boundary joining the two energy modes. Fortunately, this happens only rarely, and the cold and hot components characterizing the electron distribution function within Saturn's magnetosphere reside predominantly in the low and high energy modes, respectively. The ion and electron measurements are never made simultaneously (the shortest time difference between ion and electron spectra is 25 seconds), which may lead to time aliasing problems whenever intercomparisons between ion and electron measurements are made.

4. Large Scale Survey of Electron Observations

We present in Figure 2 a colored illustration of Saturn's magnetosphere as defined by the plasma electrons, which summarizes the results presented in this paper. The color code is such that cooler regions are bluer and hotter regions are redder. The left-hand side is a composite view of the observations near the noon meridian, while the right-hand side is more characteristic of observations in the dawn-midnight quadrant. The different plasma regimes, hot outer magnetosphere, extended plasma sheet and inner plasma torus, and other features of interest to be discussed are indicated.

An overview of the observations is given in Figure 3 for Voyager 1, and Figure 4 for Voyager 2; moment estimates of the total electron density and temperature are plotted versus dipole L. To assist in our discussions about the electron data, derived scale height information is also contained in both figures; we begin this section by discussing the centrifugal confinement of the plasma within Saturn's magnetosphere.

Like Jupiter, Saturn is a fast rotating planet and the centrifugal force will tend to confine the plasma near the equatorial plane. If the Mach number for the azimuthal flow is large enough, the plasma will form into a thin sheet centered on that plane. The vertical thickness of the plasma sheet relative to the equatorial plane can be approximated by the density scale height

$$H_i = \sqrt{\frac{1}{3}\left(\frac{Q_i}{E_i}\right)(T_e+T_i)} \simeq \sqrt{\frac{Q_i}{A_i}\left(\frac{T_e+T_i}{1.5}\right)R_s} \qquad (1)$$

originally derived by Gledhill (1967). This expression, which assumes a dipolar magnetic topology, plasma corotating at the angular velocity Ω_S reported by Kaiser et al. (1980), and ion species with mass number A_i, charge state Q_i, and corotational energy $E_i = 1/2\ A_i\ m_p\ (\Omega_s R)^2$ with m_p the proton mass, can be estimated by using the observed electron temperature T_e (in eV) and setting $T_e = T_i$, where T_i is the ion temperature.

To a zeroth order approximation one can express the Z dependence of the ion density with the expression for a single ion component plasma where the ratio $Z/H_i << 1$ (Gledhill, 1967). The expression is as follows:

$$n_i(L,Z) \simeq n_i(L,0)e^{-(Z/H_i)^2} \qquad (2)$$

where we have implicitly included the L dependence. From Eq. 2 it is readily evident that the dimensionless ratio Z/H_i determines the displacement of the spacecraft from the equatorial plane in units of the density scale height H_i of the ith ion. Therefore, Figures 3 and 4 contain both the inferred scale height H_i and the ratio $|Z|/H_i$ for singly ionized oxygen O^+ (left-hand scale) and protons H^+ (right-hand scale). Our choice of ions has been made to conform to the interpretation of the positive ion data by Bridge et al. (1981) and Lazarus and McNutt (1983) who find the plasma in the outer magnetosphere, L>10, to be nearly corotating at the rate observed by Kaiser et al. (1980) if the composition is chosen to be H^+ for the light ion and O^+ for the heavy ion. We point out that, since the scale height is inversely proportional to the energy per charge (E/Q) of the ion as indicated in Equation 1, the computed scale heights are independent of the mass assignment of the peaks in the ion spectra.

The computed scale heights in Figures 3 and 4 only reflect the spatial distribution of the cold ions, whenever they are present, where we have assumed $T_e \simeq T_{ci}$ the temperature of the cold ion component. When the cold ions are absent, the computed scale heights are underestimates of the hot

ion scale heights, since the hot ion temperature, $T_{Hi} >> T_e$ (see discussions in section 5). The principal restraining force for the hot ions is the magnetic mirror force. Throughout the remaining text, whenever we refer to the scale height H_i, we mean the scale height of the cold heavy ion component, which may or may not be O^+. The scale height H_i will pertain to the light ions, which could be H^+, only when we explicitly say so. The words thermal and cold will be used interchangeably throughout the text, whenever we are referring to the thermal electrons. The same is true for the words suprathermal and hot used to describe the suprathermal electrons.

From Figures 3 and 4 and Equation 2, it is evident that $|Z|/H_i$ can be $>>1$ at times for heavy ions, but $\lesssim 1$ for light ions at all times. Therefore, whenever $|Z|/H_i >>1$ for heavy ions, the composition is expected to be dominated by light ions; for $|Z|/H_i \sim 1$ the light and heavy ions may be of comparable abundance; while for $|Z|/H_i << 1$ heavy ions may dominate the composition. Although, this identification makes assumptions about the composition of the ion sources, the ion data presented by Bridge et al. (1982) and Lazarus and McNutt (1983) does support this compositional interpretation. Based upon these arguments, we have indicated in the bottom panel of Figures 3 and 4 those regions identified to be dominated by either light or heavy ions. For Voyager 2 the composition is expected almost always to be dominated by light ions, except at the ring plane crossing near closest approach. In the case of Voyager 1, heavy ions are expected to be dominant outside L=9 inbound and outside L=5 outbound.

Voyager 1

During the Voyager 1 inbound trajectory (noon local time) from the last magnetopause crossing at L=22.7 to the outer boundary of the extended plasma sheet at L=15, the electron density and temperature are highly time dependent. Typical densities range between $0.01/cm^3$ and $0.1/cm^3$ while the electron temperature ranges from 100 eV up to 700 eV; in Figure 2 this region is labeled as the hot outer magnetosphere. The large density spike and corresponding sharp drop in temperature at L=20 is caused by the spacecraft's close encounter with Titan. The density enhancements on

either side have been interpreted by Eviatar et al. (1982) to be Titan's "plume", an extension of Titan's comet-like tail that has been wrapped many times around Saturn by the rotating magnetospheric plasma. Referring to the lower panel in Figure 3 and trajectory plot in Figure 1b, we see that the trajectory is near the equatorial (ring) plane where the ratio $|Z|/H_i$ for heavy ions is much less than one. The large scale feature in the density profile extending from L=15 to L=7 inbound and L=7 to L=11 outbound is the extended plasma sheet, as originally defined by Bridge et al. (1981) and located in Figure 2. As the spacecraft approaches Saturn, the density within the extended plasma sheet rises with some variability from $0.2/cm^3$ at L=14 to $2/cm^3$ at L=7 with about a $1/L^4$ dependence (Bridge et al., 1982). At the same time the electron temperature decreases from ~100 eV at L=14 down to 10 eV at L=7. Similar L dependence for the density and temperature are observed during the outbound pass. The temperature drop within the plasma sheet during the inbound pass (reduction in H_i), as the spacecraft moves away from the equatorial plane (increase in Z), combine to increase the ratio $|Z|/H_i$ from 0.25 at L=16 to more than 2.0 just outside L=7 where the spacecraft is more than one scale height from the ring plane. During the outbound pass, within the extended plasma sheet, the plasma becomes warmer (increased scale height) as the spacecraft moves away from Saturn and the equatorial plane; outside L=11, the outer boundary of the extended plasma sheet and inner boundary of the hot outer magnetosphere, the plasma becomes very hot and tenuous; cold plasma is absent, and suprathermal electron fluxes less. The temperatures are such that the ratio $|Z|/H_i$ is small throughout the outbound period, except for the density enhancement near L=20, where the plasma is locally cooler. In this hot outer region the densities are less than $0.01/cm^3$; the temperature approaches 1 keV, similar to that seen outside L=15 inbound. Many of the data gaps are due to the difficulty in determining densities less than $.01/cm^3$, and at times interference is a problem and accounts for many of these gaps. A most prominent feature is the density enhancement centered on L=20, with peak densities approaching $0.1/cm^3$. This feature probably has no association with Titan, since Voyager 1 is moving down Saturn's tail at this time, at 0330 local time, well off the equatorial plane; a dipole model is misleading as to where the plasma is magnetically connected to the equatorial plane.

Inside L=7 is the inner plasma torus as defined by Bridge et al. (1982); the electron temperature there is considerably cooler than is found within the extended plasma sheet and hot outer magnetosphere. Referring to Figure 3, just outside L=7 inbound the density and temperature are decreasing with time; we then have a gap from L=7 to L=5.8, within which the L shell of Dione is situated. Within this region, the temperature of the cold electrons, T_c, is probably less than 3 eV, which makes the analysis uncertain (see following discussions on Voyager 2 data inside L=7). Near closest approach the temperature (T_e=4 eV) is observed to be a local minimum at L=4.8, very near the Tethys L shell. This minimum in electron temperature may result, in part, from a pressure anisotropy ($T_\perp > T_\parallel$), observed as a result of the changing orientation of the D sensor with respect to the magnetic field during this time. But the main reason for this reduction in temperature is an increase in cold plasma relative to hot plasma (see sections 6 and 7). The low electron temperatures observed near the Dione and Tethys L shells suggest that Dione and Tethys have a cooling influence upon the plasma.

Because of the lower temperatures, the inner plasma torus is considerably thinner (Figure 2) than the extended plasma sheet, such that the ratio $|Z|/H_i$ is at times greater than 3. After closest approach the spacecraft, which is about 2 R_S below the equatorial plane, moves toward the ring plane, and crosses it at L=6.3 ($|Z|/H_i$=0). During this time the density and temperature are rising; around L=5.5 the density maximizes at about 20/cm^3, but the temperature continues to rise. The electron temperature displays a local time asymmetry inside L=10, similar to that observed in the more energetic particle data as reported by Krimigis et al., (1983), who find the electron fluxes to be higher during the outbound pass than that observed during the inbound pass at the same L.

We note that during the UV occultation periods the spacecraft may have charged to a negative potential. (The density minimum centered on L=4.8 outbound occurs during Saturn-Sun UV occultation). In regions of shadow, the electron density will tend to be underestimated, and comparison between nearly time coincident ion and electron spectra indicate this to be so.

Therefore, the maximum density may be as high as $40/cm^3$ as reported in Lazarus and McNutt (1983). Also, the total temperature T_e will tend to be overestimated in the UV occultation regions; because the partial pressure contributed by the cold electrons P_c will be underestimated relative to that contributed by the hot electrons P_H.

Voyager 2

The Voyager 2 data in Figure 4 display a similar but more symmetric density profile. Again the plasma in the hot outer magnetosphere at noon local time is highly time dependent from the inbound magnetopause crossing (L=20.5) to the outer boundary of the extended plasma sheet (L=13). As with Voyager 1, the temperature is highly variable, and ranges from 50 eV to as high as 800 eV. No prominent density spike is present; the Voyager 2 spacecraft did not come close to Titan, which was probably within the magnetosheath at this time. The density enhancements in this variable region could be plumes or detached "blobs" of plasma which have broken off from the outer boundary of the extended plasma sheet, as argued by Goertz (1983). The spacecraft approached Saturn at high magnetic latitudes, and was more than 6 Rs above the equatorial plane at L=20. This accounts for the large $|Z|/H_i$ ratios within the cooler density enhancements. The gradual drop in $|Z|/H_i$ with decreasing L outside L=13 is attributed to the spacecraft approaching the ring plane. Considering how far the spacecraft is from this plane, it is evident that the plasma sheet has a considerable thickness.

The extended plasma sheet is observed from L=13 to L=7 inbound and L=7 to beyond L=25 outbound, remaining intact beyond L=25 in contrast to Voyager 1, which observed it to terminate at L=11. The density displays about a $1/L^4$ dependence like Voyager 1 (Bridge et al., 1982), both inbound and outbound; on the outbound leg this L dependence is obeyed all the way out to L=25. Within the extended plasma sheet at local noon the electron temperature drops from 100 eV at L=13 to 10 eV at L=7; in contrast to Voyager 1 the temperature is highly variable between L=10 and L=5.5. Outbound, the temperature rises from 20 eV at L=7 to 100 eV outside L=10, after which it is very steady all the way out to L=25 where it approaches

200 eV. Within the extended plasma sheet the ratio $|Z|/H_i$ is generally $\gtrsim 1$ inside L=10, with much variability between L=5.5 and L=10 inbound. Outside L=10 outbound, $|Z|/H_i$ steadily rises, since the temperature is relatively constant and the spacecraft is moving away from the ring plane as it recedes from Saturn.

Inside L=7, the cold electron temperatures, like those measured by Voyager 1, can fall below 3 eV; so that, as noted above, the analysis can become very uncertain. The drop in density at high latitudes inside L=6 inbound is supported to some degree by the ion data (Bridge et al., 1982); but as a result of the cold electron component's gradual disappearance from the energy spectra with decreasing L, as discussed below, the drop in density is probably not as severe as suggested by the electron data. Inside of L=4.4 inbound, where electron densities are observed to be $\lesssim 0.05/cm^3$, the rise in temperature from 4 eV to 10 eV is caused by the complete disappearance of the cold electrons in the energy spectra, illustrated by Figure 5. The cold electron component can be distinguished from the hot electrons by the break in the spectrum at E_B where there is a distinct sudden change in slope from a steep spectrum at energies less than E_B to a flatter spectrum at energies greater than E_B. As can be seen the break in the spectrum moves to lower energies with decreasing L such that the cold electron component moves to energies less than the instrument's low energy (10 eV) cutoff. This loss of cold electrons could result from two different effects. Firstly, because of the very low temperatures the cold electron component, although present at the spacecraft, becomes increasingly confined to energies less than the instrument's 10 eV low energy cutoff as it becomes colder with decreasing radial distance. Secondly, as the temperature and correspondingly the scale height drop with decreasing radial distance, the cold electrons become increasingly concentrated at lower Z coordinates than the spacecraft. In both cases the sampled fluxes reflect the hot electron component, which can reside at higher magnetic latitudes; the smaller $|Z|/H_i$ ratios computed inside L=4.5 inbound and outbound are low because they reflect only this hot electron component. Further in, between L=3.2 inbound and L=4 outbound when the instrument was in a lower sensitivity configuration, all signal was below instrument threshold. A brief enhancement (less than 96 seconds) of keV

electrons well above signal threshold at 238 0445:30 SCET at the Mimas outbound L shell crossing is the only exception. Within the gap no electron fluxes were observed during the ring plane crossing at L=2.88 where O^+ densities were estimated to be $\sim 100/cm^3$ (see inner plasma torus section where we resolve this apparent discrepancy). When the cold electrons are confined to energies near or below the instrument's 10 eV cutoff the difficulties of analysis can be largely resolved by considering the combined ion and electron data sets. This will be carried out in the future.

The general trend of the data near Tethys' L shell inbound is similar to that displayed in Figure 5, with $T_c \sim 3$ eV. Centered on the outbound crossing of Tethys' L shell at L=4.9, a sharp drop in the electron temperature to as low as 1 eV is observed. Inspection of Figure 4 shows a minimum in the electron temperature near the L shell of Dione both inbound and outbound, though not as low (T_e=7 eV) as found near Tethys. The inbound crossing of Dione's L shell gives convincing evidence that the plasma is locally cooler near Dione, though not as cold as that observed during the Voyager 1 inbound crossing of Dione's L shell. The interpretation of the drop in electron temperature near the outbound Dione L shell crossing is complicated by two factors: (1) the spacecraft underwent a roll maneuver during this time and the temperature changes may result from a pressure anisotropy and (2) the LECP instrument was stepping at a 6 second rate during the roll maneuver and interference in the PLS instrument was definitely at a higher level during this time. This interference does not appear to have affected the E1 measurements (cold component), but a significant reduction in signal because of interference seems to have occurred in the E2 measurements (hot component) at this time. There is evidence for a reduction in the temperature of the cold electrons, and whenever the cold electrons are colder the flux levels of the suprathermals are also lower. Therefore, there is a qualitative indication of a reduction in the total electron temperature near Dione's L shell, but this cannot be made quantitative. Combined, the Voyager 1 and 2 data sets indicate a localized reduction in T_e near the satellite L shells of Tethys, Dione, and possibly Rhea and that the inner satellites produce a localized cooling of the plasma within the magnetosphere.

5. Hot Outer Magnetosphere: Highly Time Dependent Region (Local Noon)

Anti-correlation of Electron Density and Temperature

In the highly time variable region of the outer magnetosphere at noon local time, the electron temperatures are very high compared to other parts of the magnetosphere. We have chosen to call this region the hot outer magnetosphere (see Figure 2), analogous to a region found in Jupiter's outer magnetosphere which is also dominated by hot plasma. The temperature variations, when studied under an expanded time scale as shown in Figure 6 for Voyager 2, are clearly anti-correlated with the density variations. In the case of Voyager 1 the density changes are most prominent near the outer boundary of the extended plasma sheet at L=15 noon local time. For Voyager 2 this spiky structure is seen throughout most of the inbound region from the plasma sheet outer boundary at L=13 to the magnetopause. The density and temperature can change by more than an order of magnitude in time periods less than 96 seconds (the sampling time of the instrument). Considering the spacecraft motion alone these brief events translate to spatial dimensions less than 1600 km or 0.027 R_S; if convected past the spacecraft at corotational speeds of 150 km/s, the dimensions become $\sim$15000 km or 0.25 R_S. This spiky structure, where n_e and T_e are anti-correlated, is similar to that seen in the outer and middle magnetosphere of Jupiter (Scudder et al., 1981). At Jupiter, the density enhancements with corresponding reductions in electron temperature are produced by the sudden appearance of cold plasma with only modest changes displayed by the hotter keV suprathermal electrons. In the case of Jupiter, this cold plasma was associated with the thin plasma sheet, for which Io was suggested to be the primary source. We now show that the density enhancements at Saturn, like Jupiter, are the result of sudden appearances and disappearances of cold plasma with only modest changes in the suprathermals.

Spectral Characteristics

In Figures 7 and 8 we display sample electron speed distribution functions (or spectra) for Voyagers 1 and 2 respectively, measured at the

time density spikes are observed. In each figure two speed distributions are displayed, measured only 192 seconds apart for Voyager 1 and 96 seconds apart for Voyager 2, at locations 1 and 2 in Figures 3 and 4, respectively. For purposes of comparison, we chose the Voyager 1 electron distributions measured most nearly time coincident with the ion spectra shown in Figures 1 and 2 in Eviatar et al. (1983). The sample electron distributions show the large variability in phase density of the cold electrons, while the suprathermal component typically shows a smaller change in phase density with the appearance of cold plasma; a similar behavior is displayed by the ion data. For the Voyager 2 electron spectrum (squares) the cold component is nearly absent, such that random fluctuations with amplitudes near instrument noise are evident in the speed distribution below 140 eV. As noted above, these distributions are reminiscent of those found within Jupiter's magnetosphere, where electrons are clearly far removed from thermal equilibrium. A single Maxwellian distribution, which has a concave downward parabolic shape in these plots, cannot adequately describe the shape of the observed distributions over the full energy range. The suprathermals themselves are non-Maxwellian since a power law in electron speed gives a better representation of their energy dependence than a parabola. The nonthermal character of these speed distributions is underscored by the fact that the suprathermal electrons contribute only 20% of the electron density, while producing more than 85% of the electron pressure (referring to Figures 7 and 8, $n_H/n_e \sim 0.20$ and $P_H/P_e \sim 0.85$ where n_H and P_H are the density and pressure, respectively, of the suprathermal electrons). A similar partitioning of density and pressure was seen in the outer magnetosphere of Jupiter (Scudder et al., 1981).

Focusing our attention on the thermal or cold electrons alone, we see from the superimposed Maxwellian fits (dashed curve) that they are well described by a Maxwellian. Using the density and temperature estimates of the cold electrons, we estimate time scales for making their distribution function Maxwellian by Coulomb collisions to be about 4 days for the Voyager 1 spectrum and 46 days for the Voyager 2 spectrum. Considering that time scales for radial transport (see Krimigis et al., 1981, who have reported a diffusion speed of 20 m/s near the orbit of Rhea) are on the order of 30 days for transport over a radial distance of 1 R_S, one expects

the cold electron distribution functions to be Maxwellian in shape if the plasma is transported over scale lengths greater than a few R_S.

The Voyager 1 ion spectra reported by Eviatar et al. show that the appearance of the denser cold electrons is associated with the appearance of cold ion peaks in the D sensor, indicating a high mach number azimuthal flow moving in the corotation direction. Lazarus and McNutt (1983) find that the composition H^+ and O^+ is consistent with the plasma moving nearly at, but below, corotation speeds. When the total charge density contributed by the cold ions is compared with that estimated for the cold electrons, one finds the electron density is about a factor of 2 less than that of the ions. Since the cold plasma density is changing rapidly with time and the electron density is intermediate in value between the ion densities measured before and after it, consistent with a rising trend in the density, the ion and electron measurements are not necessarily in disagreement with each other. When one compares the ion and electron densities over a longer time interval, they are in agreement within about 30%. It is also evident that when the hot ion fluxes decrease, the hot electron fluxes above 100 eV also decrease. (Note that Lazarus and McNutt refer to the hot ions below 6 keV as the warm ion component.) The above suggests an association between the cold (hot) ions and cold (hot) electrons. A visual survey of the ion, electron spectra for the full encounter data set support this association. The ion and electron spectra at this time show the ion temperature to be about 5 times greater than the electron temperature, and that the warm ion component contributes most to the plasma pressure.

6. Extended Plasma Sheet

Spectral Characteristics

As found within the density enhancements outside L=15, the plasma electrons within the extended plasma sheet are again composed of a cold and a hot component. Throughout most of the extended plasma sheet the suprathermal or hot electrons dominate the electron pressure, while the thermal or cold electrons dominate the density. The positive gradient in

electron temperature between L=7 and L=12 (cf. Figure 3, 4) has a number of causes as illustrated in Figures 9 and 10, where we have displayed sample spectra observed within the extended plasma sheet by Voyager 1 and 2, respectively; the positions of the measurements are indicated by numerals 3 and 4 in Figure 3 for Voyager 1 and numerals 5 and 6 in Figure 4 for Voyager 2. As can be seen, the energy spectrum of both cold and hot components separately become increasingly steeper on average with decreasing radial distance. Also, the cold electrons contribute more to the density and pressure at smaller L, than the hot electrons. Near the outer boundary of the plasma sheet, the suprathermal electrons contribute nearly 25% to the density, and more than 80% to the pressure. In contrast, near L=7 at the inner boundary, the suprathermals contribute less than 10% to the density, and less than 50% to the pressure. This reduction in fractional density and temperature of hot electrons is caused, in part, by the suprathermal electrons being depleted as they are transported inward, and that this depletion is greater at higher electron energies. We later show that this energy dependent depletion is probably caused by an interaction with neutral material or wave-particle interactions within Saturn's inner magnetosphere.

Cold, Hot Partitioning of Electron Density and Pressure

To demonstrate the large scale validity of these spectral changes, 5 minute averages of the fractional density n_H/n_e and pressure P_H/P_e contributed by the suprathermal electron component are plotted in Figure 11 (see Sittler (1983) for details). In the outer magnetosphere, where electron temperatures approach 1 keV, the suprathermals can occupy more than 50% of the density and nearly 100% of the pressure; in denser regions these ratios are typically ~20% and 80%, respectively. At the outer boundary of the extended plasma sheet at local noon, there is an abrupt drop in the density ratio for both spacecraft. This follows from our original statement that the plasma sheet is primarily composed of cold plasma. The plots of P_H/P_e show that the suprathermal electrons continue to dominate the pressure within the extended plasma sheet; it is only inside L=10 that we see their importance diminishing. The inner boundary of the extended plasma sheet and outer boundary of the cold inner plasma

torus are clearly defined by the abrupt drop in the suprathermal electron density and pressure ratios inside L=7 for both encounters. The brief rise in the pressure ratios inside L=6 inbound for Voyager 1, and near L=6 outbound for Voyager 2 are temporary recoveries of the suprathermal electrons relative to the cold electrons. We emphasize, that in these regions the computed temperature of the hot component can be as low as 10 eV.

The ratios of n_H/n_e and P_H/P_e may be anomalously high in the Voyager 1 data between L=4.4 and L=5.75 outbound, because of UV occultation by Saturn and its rings which may cause the cold density to be underestimated as a result of a negative spacecraft potential. Within the hot outer magnetosphere, in regions where the cold component is absent, the analysis will fit a Maxwellian to the low energy portion of the suprathermal component and interpret it as the cold electron component. When this happens, typical temperatures for the low energy Maxwellian fit are $\gtrsim$ 100 eV and $\sim$50% of the density will be in this component (see Figure 8). Under these circumstances, an estimate for n_H/n_e $\sim$50% may in reality be as high as 100%.

In the Voyager 1 outbound data, outside L=11, the coverage is very poor because, as mentioned before, of interference problems in the higher energy channels. A visual scan of the data clearly shows the total lack of a cold component in the energy spectra. The densities are very low ($n_e < 10^{-2}/cm^3$) and temperatures are high ($T_e \sim 1$ keV). The reduction in partial pressure for the suprathermal electrons displayed by the Voyager 2 outbound data outside L=10 (P_H/P_e is a maximum at L=10) is presently not fully understood. As pointed out before, the data suggests a relationship between the hot ions and hot electrons and that, for the spectrum in Figures 1 and 2 in Eviatar et al. (1983), the hot ions dominate the ion pressure. If the ions display a similar partitioning in pressure between their cold and hot components like the electrons, then the hot ions should dominate the ion pressure within the extended plasma sheet.

7. Cold Inner Plasma Torus

As described in section 4 and illustrated in Figure 2, the inner plasma torus is a region of reduced electron temperature and scale height. This reduction in temperature, similar to that observed within the extended plasma sheet inside L$\sim$10, is caused by a cooling of the cold electrons and significant depletion of the suprathermal electrons. We begin this section with a re-evaluation of the preliminary interpretation of the Voyager 2 ring plane crossing data presented in Bridge et al. (1982) from which it becomes evident that the electron temperature can be as low as 1 eV within the inner plasma torus.

Voyager 2 Ring Plane Crossing: $T_e \lesssim 1$ eV

In Bridge et al. (1982), it was noted that the observed thickness of the plasma sheet of 0.2 R_S at L=2.88 was considerably less than one would estimate using the observed temperature of 10 eV for O^+ ions, setting $T_e=T_{O^+}$ and using Eq. 1; doing this they estimated $H_i=0.9$ R_S. A pressure anisotropy in the ions was the proposed explanation for this inconsistency, but the required pressure anisotropy $P_\perp/P_\parallel \sim 20$ is very large. Coulomb time scales for isotropization of O^+ ions, with densities $\sim 100/cm^3$ and temperatures ~ 10 eV, are on the order of 30 days (see Rossi and Olbert, 1970). The residence times are at least this large, hence it seems inconceivable that this is an appropriate explanation. During the ring plane crossing, the electron temperature is at such a low level that the thermal electrons are confined to energies below the instrument low energy cutoff of 10 eV. By knowing the electron density and spacecraft potential from the ion measurements, one can compute an upper estimate for T_e by setting the phase density of a Maxwellian representation of f_e equal to the minimum phase density of f_e set by the instrument signal threshold in the lowest speed channel. Using $n_e=100/cm^3$ and setting $\phi_{SC} = 0$ volts, we compute an upper estimate for $T_e=1$ eV. (Note, the spacecraft potential is probably negative at this time, so that T_e will be underestimated somewhat by setting $\phi_{SC} = 0$ volts. The ion data are inconsistent with potentials in excess of a few volts in magnitude. Finally, the effect of the negative spacecraft potential is somewhat compensated by ignoring the density

contributed by light ions). It then follows that $T_e/T_{O^+} << 1$, so that the originally estimated scale height is reduced by $\sqrt{2}$, from 0.9 R_S to 0.64 R_S. Then using the arguments developed in Lazarus and McNutt (1983), the required pressure anisotropy $P_\perp/P_\parallel \lesssim 6$ is more reasonable.

Depletion of Suprathermal Electrons

Inside L~10, the density and pressure ratios for the hot electrons, shown in Figure 11 display a large scale reduction with decreasing radial distance from Saturn. The large drop in pressure ratio is caused, in part, by a systematic attenuation of the suprathermal electrons with decreasing radial distance. In most cases, the attenuation is greatest at higher electron energies and shifts to lower energies as L decreases. Sittler et al. (1981), using Voyager 1 data originally attributed this systematic attenuation of the suprathermal electrons to interactions with Saturn's diffuse E-ring. This feature is observed to extend from L=9 inbound to L=7 outbound (Voyager 1) and L=10 inbound to L=7 outbound (Voyager 2). In both cases, this large scale depletion displays a local time asymmetry with suprathermal electron fluxes recovering closer to Saturn during the outbound pass. Examples of the attenuation, referred to as "bite-outs" are given in Figures, 5, 9 and 10. In Sittler et al., they were identified by the negative curvature, η, of the electron distribution function f_e in $\ln f_e$ vs $\ln v_e$ space at the maximum energy, E_{max}, at which the electron fluxes exceed the instrument signal threshold.

Bite-out signatures identified by PLS are apparently associated with energy dependent signatures found by LECP (Krimigis et al., 1981, 1982, 1983) in the regions from L=9 inbound to L=6.5 outbound (Voyager 1) and L=10 inbound to L=7 outbound (Voyager 2). The energy ranges are 37 to 70 keV for Voyager 1 and 22 to 35 keV for Voyager 2. When combined the two data sets suggest an energy dependent depletion of electrons which is greatest at an energy between the highest energy fluxes are measured above instrument signal threshold by PLS (E < 6 keV) and the lowest energy measured by LECP (indicated above). We discuss in section 10 the possible causes of this phenomenon.

In addition to the large scale reductions, there are localized (small scale) reductions in the suprathermal electron fluxes. Referring to Figure 12, and noting the results displayed in Figure 3 of Sittler et al. (1981), the Voyager 1 data displays a localized minimum in suprathermal fluxes centered on Dione's L shell inbound. For $L \lesssim 9$ the bite-out is confined near 6 keV, and then moves to lower energies until inside $L \sim 7$ it is confined to energies less than 50 eV. Between L=7 and L=5.5 inbound, within which Dione's L shell resides, electron fluxes above 50 eV are confined near or below instrument signal threshold (gap in Figure 12 from 317 1900 to 2200 SCET). Inside L=5.5 inbound the suprathermals display a gradual recovery and then brief reduction in flux near the Tethys L shell at $L \sim 4.9$. In the outbound data no localized depletion of hot electrons is observed near the L shells of Tethys and Dione; as shown in Figure 12 the suprathermal electron fluxes increase with increasing radial distance until they maximize near the ring plane crossing. The local minimum in density and pressure ratios centered on L=4.9 inbound and between L=4.9 and L=7 outbound, is primarily caused by an increase in cold relative to hot plasma.

The Voyager 2 inbound data displays small scale bite-out signatures extending out to nearly L=10 where the depletions are confined to energies near 6 keV. (Like Voyager 1, the depletions move to lower energies as the spacecraft moves inward). Within the highly time dependent region between L=10 and L=5.5 inbound for Voyager 2 (see Figure 4 and Figure 16), bite-out signatures in the energy spectra are observed whenever temperature minima occur. Therefore, the hot electron fluxes display a very time dependent behavior within this time interval. Similarly, Krimigis et al. (1982, 1983) reported large time dependent variations in electron fluxes with energies $\sim$30 keV within the same spatial regime. Centered on the inbound Dione L shell crossing, an enhanced depletion of suprathermal electrons lasting $\sim$40 minutes is observed. Within this feature, very near the predicted L shell of Dione (Connerney, private communication), there is a brief density enhancement with large increase in the suprathermal electron fluxes extending up to 6 keV (see Figure 16). Inside of Dione's L shell, the attenuation remains strong at smaller radial distances such that no significant fluxes above 140 eV are observed inside L=5.

The localized cooling associated with the Voyager 2 outbound crossing of Tethys' L shell is difficult to interpret because of the low flux levels above 30 eV and very steep slope in the cold electron spectrum. Present tentative analysis indicates a localized cooling, with an addition of cold plasma the most likely cause. Note that during this time the Voyager 2 spacecraft did come within 93,000 km downstream of Tethys as it crossed the Tethys L shell, so cold plasma recently loaded onto field lines may have been observed. The observed decrease in P_H/P_e during the Voyager 2 outbound crossing of Dione's L shell, occurs during the roll maneuver noted in section 4, and is therefore uncertain.

8. Association between Suprathermal Electrons and Whistler Mode Emissions

Gurnett et al. (1981) and Scarf et al. (1982), reported emissions of hiss and chorus. These whistler mode emissions appear to be associated with the presence of suprathermal electrons with which they are resonating, although emissions are observed at times when no electrons below 6 keV are detected. In Figure 3 of Gurnett et al. (1981), no whistler mode emission is apparent between 1900 and 2100 hours SCET on day 317. As shown in Figure 12, no electron fluxes of significance above 50 eV were observed during this same time period. After 2100 hours, whistler mode emission between 560 Hz and 3.1 kHz shows a steady increase with time. At 1 kHz, where the maximum intensity occurs the emission peaks at about 2300 hours, after which it decreases and the emission spreads out to a broader band of frequencies. The intensity of the broad banded emission then rises steadily with time, with a maximum near the ring plane crossing at 0414 hours on day 318. Showing a similar time dependence, the suprathermal electrons recover from below threshold flux levels starting at about 2100 hours, after which they rise steadily until near closest approach where they display a leveling off and brief drop in flux between 317 2351 and 318 0031 (predicted crossing of Tethys' L shell is 318 0012; Connerney, private communication). The hot electron flux levels then continue to rise, with a maximum near the ring plane crossing. As expected, the increase in wave emission is associated with an increase in phase density of the particles in resonance with them.

When the emission is confined to a narrower range of frequencies, for example, the time period between 317 2100 to 318 0000 hours, the hot electrons are of low density ($n_H \sim 0.01/cm^3$) and characteristically lower temperatures ($T_H \sim 100$ eV). When the whistler mode emission covers a broader band of frequencies (i.e., during the ring plane crossing), especially toward lower frequencies, the suprathermal densities ($n_H \sim 1/cm^3$) and temperatures ($T_H \sim 250$ eV) are higher. This movement of whistler mode emission to a broader range of freqencies, especially toward lower frequencies, is expected with an increase in density and temperature of the suprathermal electrons. Furthermore, during the ring plane crossing, the critical energy $E_{CR} = B^2/8\pi n_e$ is locally smaller. Because of this, waves of a given frequency will resonate with lower energy electrons. Both effects combine to enlarge the range of electron energies of sufficient phase density that are available to resonate with the waves, such that the lower frequency waves resonate with the more energetic electrons (see Kennel and Petschek, 1966). This initial survey of the Voyager 1 data, shows that there is an association between enhanced levels of whistler emission and suprathermal electron fluxes. With the Voyager 2 data, this association is not as clear. For example, the emissions displayed in the broadband data in Figures 3B and 3C of Scarf et al. (1982) must be in resonance with more energetic electrons E > 6 keV, since no suprathermals above 30 eV are observed at these times. Because at this time E_{CR} is locally greater than 100 keV and probably not less than a few keV at the equatorial plane, either of those times, it is expected that the whistler mode waves are in resonance with more energetic electrons. In summary, one can say that the observed whistler emissions can at times be interpreted to be in resonance with the low energy E < 6 keV electrons, and at other times they are probably in resonance with more energetic electrons.

9. Saturn's Ring Current

Ness et al. (1981, 1982) and Connerney et al. (1981) reported evidence of an extended ring current system in Saturn's outer magnetosphere. This model ring current, based on Voyager 1 magnetic field data, had inner and outer boundaries of 8.5 and 15.5 R_S in the equatorial plane with a full uniform vertical thickness D of 5 R_S. Connerney et al. used a 1/R dependence for the current density (R is the equatorial radial distance), which was constant between $-D/2 < Z < D/2$; for $|Z| > D/2$ the current was zero. At the inner radial boundary of the ring current, they estimated a current density $j = 3 \times 10^5$ Amp/R_S^2. In this section we explore the observational implications this model has on the plasma data and visa versa.

The currents within Saturn's magnetosphere are the result of charged particle motions brought about by gradients in the system. Currents carried by the low energy plasma (for which gyro-radii R_g are small compared to characteristic spatial scale lengths L_C for the particles and fields $R_g/L_C << 1$) are produced by stresses imposed upon the magnetic field by the centrifugal force of the azimuthally flowing plasma, pressure gradients in the plasma, electric fields and gravity; for our purposes, the electric and gravitational fields may be neglected. Mathematically, the plasma currents $\vec{j}$ are embodied in the $\vec{j}\times\vec{B}$ term in the momentum equation; by assuming rigid corotation, steady state, and azimuthal symmetry, the current density can be shown to have the following form (see for example Rossi and Olbert, 1970, page 270)

$$j_\perp = \frac{1}{Br}\left\{\rho(\Omega_s r)^2\left[\frac{\cos\lambda(1-\sin^2\lambda)}{\sqrt{1+3\sin^2\lambda}}\right] - 2\sin\lambda\ \frac{\partial p}{\partial\lambda} - r\cos\lambda\ \frac{\partial p}{\partial r}\right\} \qquad (3)$$

where λ is the magnetic latitude, we have assumed isotropy in the pressure P, and used a dipole field for $\vec{B}$. The first term is from the centrifugal force, while the other two are caused by latitudinal and radial gradients in the plasma pressure, respectively. If the term in brackets is positive, the current will flow in an eastward direction, if negative in a westward direction. We see from Eq. 3 that the radial and latitudinal dependence of $j_\perp$ is not obvious, and will depend critically upon the spatial distribution

of the density and composition (centrifugal term) and the spatial distribution of the plasma pressure (pressure gradients). Another important point about Eq. 3, is that $j_\perp$ is inversely proportional to B, which tends to make the current densities greater in the outer magnetosphere and near the equatorial plane where B is a minimum. Finally, the change in the magnetic field $\Delta\vec{B}$ produced by the ring current is given by a volume integral over the current distribution (Biot-Savart Law). Thus the change in $\vec{B}$ will be a function of the total thermal and centrifugal energy of the plasma.

The radial and vertical boundaries of the model ring current nearly coincide with that defined by the extended plasma sheet as defined by PLS; the half thickness of the ring current D/2 is approximately that defined for the cold heavy ion plasma (i.e., $H_{O^+}=2.5\ R_S$). In order to better understand this relationship between the ring current and extended plasma sheet, and to evaluate the relative importance of the contributions of centrifugal and pressure gradient terms to the ring current, it is useful to rewrite Eq. 3 in a different form. We do this by considering only the heavy ions such as O^+, assume the density decreases with a $1/R^\alpha$ dependence, assume a positive gradient in R for the temperature $T = T_e + T_{ion}$ of the plasma (i.e., T proportional to R^δ) and confine our estimates to the equatorial plane where the current densities are expected to be highest. We then get

$$j_\perp = \frac{1}{4\pi}\left(\frac{B_o}{r_o}\right) M_{Ao}^2 \left\{ \left(\frac{X_o}{X}\right)^{\alpha-4} + \frac{(\alpha-\delta)}{2} \frac{1}{M_{so}^2}\left(\frac{X_o}{X}\right)^{\alpha-\delta-2} \right\} \qquad (4)$$

where M_{AO} is the Alfvén Mach number for the azimuthal flow of the plasma at reference point $R_o=R_S X_o$, $B_o=B(R_o)$, $M_{So}^2=E_o/P_o$ is the sonic Mach number squared equal to the ratio of centrifugal energy density $E_o=1/2\ \rho_o(R_S\Omega_S X_o)^2$ over plasma pressure evaluated at R_o, ρ_o is the mass density at R_o, and $R=R_S X$. The first term characterizes the currents produced by the centrifugal force, while the second term, proportional to the plasma beta $\beta = M_A^2/M_S^2$, is caused by the pressure gradients. If $M_{So}^2 >> 1$, then the centrifugal term is the dominant contributor to the current density. If

$M_{So}^2 << 1$, then the dominant contributor to the current is the pressure term. Estimates at specific locals indicate that M_S^2 is $\gtrsim 1$ within the extended plasma sheet. In sections 5 and 6 we showed that hot ions are expected to dominate the plasma pressure in the extended plasma sheet and hot outer magnetosphere. For example, the warm ion component displayed in Figure 1 of Eviatar et al. (1983) alone gives a plasma beta ~ 1.0. The ion pressure in the LECP energy range (Krimigis et al., 1983) indicate plasma β which can exceed one between L=6 and L=9 near the equatorial plane, if the composition is O^+. Outside L=10, where the composition is probably H^+, the plasma β are $\lesssim 0.5$. So the pressure terms do appear to be competitive with the centrifugal term.

As a means of studying the general morphology of the plasma pressure measured by the PLS instrument, we display in Figure 13, plots of the electron pressure P_e and electron beta β_e versus dipole L. Concentrating our attention upon the Voyager 1 data, from which the ring current parameters were originally derived, we see that the electron pressure displays a steady decrease in L, outside L=9 for the inbound data. Outside L=15 inbound, it then levels off to a constant value on average, all the way to the magnetopause. It is interesting to note that P_e shows no variation across the magnetopause, except for small scale variations associated with the actual boundary crossings. The outbound data shows the electron pressure maximizing during the ring plane crossing at L=6.3, after which it drops off with increasing L. The turnover inside L=7 inbound is caused by a decrease in electron temperature and movement of the plasma sheet below the spacecraft position as the plasma cools. Outside L=11 outbound, where the extended plasma sheet has terminated the pressures are very low. If there is a definite association between the ions and electrons as previously discussed, and the pressure term makes a significant contribution to the ring current, one would expect the ring current to terminate at the outer boundary of the extended plasma sheet where either the gradients are weak or the medium is devoid of plasma. It should also be said that the cold ions, which contribute to the centrifugal term, also terminate outside the extended plasma sheet at about L=15 inbound.

The electron β displays an overall decrease with decreasing radial distance from Saturn during the inbound pass. In the hot outer magnetosphere β_e is $\sim$0.2, within the extended plasma sheet outside L=10 it is $\lesssim$ 0.1, while inside L=10 it displays a steep decline with decreasing L, which as noted for P_e, is attributed to a thinning of the plasma sheet as it cools and a reduction in electron temperature. The outbound profile is very similar in shape, except (1) the turn over in β_e occurs closer in at L=7.5 compared to L=10 for the inbound data, and (2) the β_e are apparently very low outside L=11, outside of which the plasma sheet terminates. Comparing the inbound and outbound electron beta observed at the same L, we see they are approximately equal at L=10, while inside L=10 the electron beta is larger during the outbound pass. This asymmetry in β_e is caused by the spacecraft being nearer the equatorial plane and the electron temperature being higher, during the outbound pass.

For Voyager 2, the electron pressures outside L=8 are comparable to the Voyager 1 pressures at the same L. Like Voyager 1 the P_e and β_e profiles turn over inside L=7; the plasma is cooler and the plasma sheet has moved below the spacecraft position. In contrast to Voyager 1, the inbound Voyager 2 P_e and β_e profiles are very mixed in structure; on average no pressure gradient is evident within the extended plasma sheet at local noon, though a lot of fine structure is present. The flatness displayed by the pressure profile is caused by the steep temperature gradient (see Figure 4) inside L=12, which offsets the $\sim 1/L^4$ decrease in the density. Because the magnetic field pressure has a strong L dependence ($1/L^6$) and P_e is nearly a constant on average, β_e shows a steep positive gradient in L inside L=12. Another major difference in the Voyager 2 data is that β_e is nearly a factor of 10 smaller for Voyager 2 than for Voyager 1. This difference is caused by the Voyager 2 spacecraft being at higher magnetic latitudes where the internal magnetic field strength is greater, and the spacecraft being above the ring current such that the current contributions to $\Delta\vec{B}$ add to the internal magnetic field. As noted before, the ring current will be largest near the equatorial plane where B is a minimum. The outbound data is more reminiscent of the Voyager 1 observations; the electron pressure displays a steady $\sim 1/L^4$ decrease outside L=8, until L=17, after which it levels off. Since the spacecraft is moving away from

the equatorial plane with increasing L, this leveling off of the pressure profile is expected to occur at smaller L near the equatorial plane where the currents are most important. (A similar argument will make the pressure profile near the equatorial plane less steep between L=13 and L=20 inbound.) So again, the ring current, if dominated by pressure gradients, will terminate for $L \gtrsim 15$. Within the inner plasma torus, the electron β are very low $< 10^{-3}$, since the spacecraft is either far off the equatorial plane (above plasma sheet) or at the ring plane crossing (L=2.88) the plasma is very cold and the magnetic field strength is high. Finally, we note that the electron pressure profiles in Figure 13 are very similar in shape, with some exceptions, to those reported by Krimigis et al. (1983) for hot ions in the LECP energy range.

To get some representative values of the total plasma beta, one can compare ion spectra which have been analyzed in detail with almost time coincident electron spectra. The electron spectrum in Figure 7 and nearly time coincident ion spectrum in Figure 2 of Eviatar et al. (1983) show the ion pressure P_i in the outer magnetosphere to be $\sim$5 times the electron pressure, and suggest that the hot ions dominate the ion pressure there as the hot electrons dominate the electron pressure. Similarly, the Voyager 1 ring plane crossing ion spectrum at 318 0408 SCET at L=6.3 (R. L. McNutt, private communication), and the almost coincident electron spectrum in Figure 14 show P_i to exceed P_e by a factor of 10. The same can be said for the Voyager 2 ring plane crossing data. Thus the presently available evidence suggests the ion pressure significantly exceeds the electron pressure and that the total plasma beta for ions and electrons below 6 keV is $\lesssim$ 0.5 to 1.0 in the extended plasma sheet, $\lesssim$ 0.25 to 0.5 within the outer parts of the inner plasma torus ($L > 6$), and $\gtrsim$ 1.0 in the hot outer magnetosphere.

Assuming the electrons give a fair description of the ion pressure profile below 6 keV, one can make a rough estimate of $j_\perp$ using Eq. 4. We will use the $1/L^4$ dependence in the pressure suggested by Figure 13; a precise value of the slope will not critically influence our estimate. We will use typical Voyager 1 plasma and field parameters at $L \sim 10$. Using B=20 nT, $P_e = 10^{-10}$ erg/cm^3, and setting $P=5\ P_e$ we estimate $\beta=0.4$. The

Alfvén Mach number with a density of 1.0/cm^3, assuming O^+ ions, and assuming corotation speed of 100 km/s, is M_A=0.92 and the sonic Mach number squared M_{So}^2 = 2.1. Substituting into Eq. 4, we estimate $j_\perp$ = 1.4 x 10^5 Amp/R_S^2, which is within a factor of 2 of the estimated $j_\perp$ = 2.5 x 10^5 Amp/R_S^2 by Connerney et al. (1981) at L=10. These calculations, similarly done by Lazarus and McNutt (1983), demonstrate that the low energy plasma does contribute to a significant fraction of the ring current. For this particular estimate, the pressure term contributes to about 50% of the current. Although more precise estimates of the plasma beta and pressure gradients (PLS and LECP) are required to make a definite statement about the relative importance of the centrifugal and pressure gradient terms, it does appear that the pressure gradient term is competitive with the centrifugal term in the estimation of $j_\perp$.

Ness et al. (1982) reported significant deviations between the outbound Voyager 2 magnetic field measurements and predictions by the Connerney et al. (1981) model based on Voyager 1 observations. The suggested explanations were temporal variations in the solar wind momentum flux between encounters or neglect of magnetotail currents. We offer an alternative explanation, in that the extended plasma sheet was observed to extend beyond L=25 during the Voyager 2 outbound period, while for Voyager 1 the plasma sheet terminated outside L=11 outbound. (We note that a similar behavior is displayed by the LECP data reported by Krimigis et al. (1983)). The presence of the plasma sheet beyond L=25 for Voyager 2 produces a definite enhancement of the ring current within the dawn-midnight quadrant relative to that present during the Voyager 1 outbound pass. One can see from Figure 2 in Connerney et al. (1981), that deviations between the model calculations and the magnetic field measurements occurred between ~16:30 and 19 hours on day 317 and between 6 and 8 hours on day 318. The inbound anomaly can probably be attributed to ignoring the presence of a ring current inside L=8.5 which is confined nearer the equatorial plane. The latter anomaly is probably caused by a somewhat thicker ring current during the outbound pass than that used in the model calculations.

10. Summary and Discussion

The survey of the low energy plasma electron observations made at Saturn by the Plasma Science Experiment (PLS) during the Voyager 1 and 2 encounters, shows the electrons, like the ions (Eviatar et al., 1983; Lazarus and McNutt, 1983), to be composed of a cold and a hot component. The cold (thermal) electrons display a Maxwellian energy dependence, while the hot (suprathermal) electrons have a non-Maxwellian energy dependence. This two component structure characterizing the electron distribution function, was also seen in Jupiter's magnetosphere (Scudder et al., 1981). Residence times for the trapped cold electron component are probably long enough to allow Coulomb collisions to make them nearly Maxwellian; the hot electrons evidently are too hot and tenuous for Coulomb collisions to have a significant effect on them. There is evidence in the speed distributions for a filling in of the spectrum at the breakpoint energy E_B separating the cold and hot components; as discussed below Coulomb collisions are probably the cause of this. The data also suggests a possible association between the cold (hot) electrons and the cold (hot) ions.

A striking overall feature of the plasma electrons is the large decrease in electron temperature with decreasing radial distance, from $\sim$800 eV in the outer magnetosphere to less than 1 eV in the inner magnetosphere. In regions within the outer magnetosphere where cold plasma is present the computed scale height for the cold heavy ions is $\sim$3 R_S, while within the inner magnetosphere the observed scale height at L=2.88 is 0.2 R_S (Bridge et al., 1982). This drop in plasma sheet thickness by more than an order of magnitude can mainly be attributed to the drop in plasma temperature with decreasing radial distance, although changes in composition and pressure anistropy may also contribute. We suggest three possible causes for this decrease in electron temperature: 1) a source of cold plasma within Saturn's inner magnetosphere combined with heating and outward transport; 2) a plasma source in the outer magnetosphere combined with cooling and inward transport; or 3) both mechanisms are in effect. We presently feel the third choice is most consistent with the plasma data as a whole, with the first effect primarily influencing the thermal electrons, and the second the suprathermal electrons. The suprathermal electrons

dominate the electron pressure in the outer magnetosphere, while the thermal electrons become dominant within the inner magnetosphere near the equatorial plane; within the inner magnetosphere the hot electrons may also dominate the electron pressure at high latitudes. From the measurements one can identify three distinct plasma regimes as illustrated in Figure 2: 1) the hot outer magnetosphere, 2) the extended plasma sheet, and 3) the inner plasma torus.

Hot Outer Magnetosphere

The hot outer magnetosphere is that region residing between the outer boundary of the extended plasma sheet and the magnetopause. Throughout this region the suprathermal electrons dominate the electron pressure. In the midnight-dawn quadrant of the outer region the densities are usually $< 0.01/cm^3$, and the electron temperatures > 500 eV. Near the noon meridian both density and electron temperature show a highly variable behavior, with anti-correlated density and temperature variations. The density enhancements are caused by the sudden appearance of cold plasma; order of magnitude changes can take place in less time than the sampling period of the PLS instrument (96s). Density is observed to vary between $0.01/cm^3$ and $0.1/cm^3$, while the temperatures vary between 50 eV and 800 eV. In the low density, high temperature regions cold plasma is absent and all the density and pressure is contributed by the hot electrons. Within the density enhancements the cold electrons can dominate the electron density ($n_H/n_e \sim 20\%$), but the hot electrons continue to dominate the electron pressure ($P_H/P_e \sim 80\%$). In this outer region the plasma β is probably greater than one, but on average the pressure gradients are very weak (spatial scales greater than 1 R_S).

Hot Plasma Source

Eviatar et al. (1983) have suggested that the source of warm ions observed below 6 keV by the PLS instrument in the outer magnetosphere, is the local ionization of neutral gas within Saturn's rotating magnetosphere. The atomic hydrogen cloud (Broadfoot et al., 1981; Sandel et al., 1982) can account for the warm hydrogen component reported in their paper. To

account for the heavy ion constituent of the warm plasma a heavy neutral not yet detected, must be present in sufficient quantities within the neutral cloud. Eviatar et al. have suggested atomic nitrogen emitted by Titan by way of exoenergetic dissociative reactions of molecular nitrogen (Strobel and Shemansky, 1982). They also suggested emission of atomic oxygen to the outer magnetosphere by the main rings. Charge exchange reactions between a corotating ion and an ambient neutral will produce a fast neutral which does not have sufficient energy to escape the Saturnian system and is confined to Keplerian orbits residing within the vicinity of the neutral hydrogen cloud. After ionization, these newly born ions are accelerated by the motional electric field and form cycloidal distributions comoving with the rotating magnetospheric plasma with gyro-speeds equal to the azimuthal speed of the locally rotating plasma. These distributions, which are unstable to the generation of plasma waves (Wu and Davidson, 1972), are expected to become thermalized to form a Mach 1 plasma. For the specific case presented in Eviatar et al. (1983) the hot component is observed to be a Mach 1 plasma, as required, with the temperature of the O^+ (or N^+) hot ion being 1.3 keV.

The source of the suprathermal electrons is not so clear, since electron pick up energies are confined below 1 eV within Saturn's magnetosphere. Therefore, some other mechanism must be present to account for the hot electrons which have a mean thermal energy ~100 to 300 eV for the electron spectra displayed in Figures 7 and 8. One viable possibility is the double exobase concept proposed in Scudder et al. (1981) for Jupiter.

Cold Plasma Density Enhancements

The source of the density enhancements in this chaotic plasma regime in the noon sector is presently unresolved. Eviatar et al. (1982) have presented convincing evidence that the Voyager 1 density enhancements (L=21 and L=19.2) on either side of the main Titan encounter plume at L=20 are remnants of Titan's plume or cometary tail; the density enhancement at L=18 is less convincing. The change in position of the plumes relative to L=20, was attributed to the compression and expansion of the magnetosphere,

which is responding to changes in the external solar wind pressure. The observations are consistent with a gradual aging of the plumes, characterized by a dispersal of the plumes by the centrifugal interchange instability, heating and acceleration. An aging effect was also suggested by Sittler et al. (1981), who studied bite-out signatures in the suprathermal electron tails as an indirect indicator of the presence of neutral material. Within the main Titan plume, a strong attenuation of the suprathermal electrons above 700 eV (bite-out) was observed (Bridge et al., 1981). As the plume age increased, the bite-out signatures became degraded (turn over in the spectrum moved to higher energies); for the oldest plume at L=18 the signature is nearly absent. The time scale for plume dispersal, at which point they become indistinguishable from the background plasma, was estimated to be on the order of a few Kronian rotation periods.

Goertz (1983) presented a different interpretation, in which the chaotic region is called a "turbulent layer", which may not necessarily contradict the plume identification made by Eviatar et al. (1982). The density enhancements are "blobs" of plasma which have become detached from the outer boundary of the extended plasma sheet by the centrifugally driven flute instability. This model is motivated by the flat top shape of the density enhancements, and because the amplitude of the density enhancements display the same L dependence as the density within the extended plasma sheet. For the Voyager 1 data in Figure 3, from which Eviatar et al. presented evidence for Titan plumes, the model by Goertz does not appear to be supported, except near the plasma sheet outer boundary between L=16 and 17. For Voyager 2, Titan was apparently in the magnetosheath or near the magnetopause boundary (P. Gazis, private communication) for a few days (estimated plume lifetime) before the spacecraft entered the magnetosphere. Therefore, one does not expect to see any evidence of plumes, which may also be confined nearer the equatorial plane. So, it is not surprising to see no clear evidence of plumes in the Voyager 2 data, which appears to support the Goertz model from the outer boundary of the extended plasma sheet all the way to the magnetopause.

A completely different interpretation has recently been presented by Lazarus et al. (1983) for some of the plasma sheet associated density

enhancements. When they overlaid the Pioneer 11 and Voyager 1 and 2 dipole L shell plots of the density between L=14 and L=17, Lazarus et al. found a remarkably good match between them; the density maxima and minima were lined up quite well. They argued against the detached plasma model, since the detached plasma "blobs" should be randomly distributed in L, and proposed ring absorption as the cause of density depletions. One problem with this model is that plasma cannot diffuse across the ring zone without being depleted; hence if there is outward transport, the density enhancements outside the plasma sheet should be absent.

Because of the large ion pick-up energies at this radial distance, the neutral cloud is a source of hot plasma. Similarly protons from Saturn's ionosphere will acquire large field aligned flow energies $\gtrsim$ 100 eV at L$\sim$15 (see Hill et al., 1974). Such large field aligned flows for cold H^+ ions are not observed (Lazarus and McNutt, 1983), and therefore the ionosphere is probably a source of warm plasma at these large radial distances (i.e., field aligned flow energy thermalized). The density enhancements are principally composed of cold plasma, and are thus not formed by ionization of Saturn's neutral cloud or locally deposited ionospheric plasma. The most likely sources of cold plasma are; (1) Titan's plumes, (2) ionization of neutral gas within the inner magnetosphere and (3) ionospheric plasma deposited in the inner magnetosphere. The lack of any significant ring signature in the Voyager 2 outbound data, where the extended plasma sheet is intact all the way to L=25 may not be a problem for the Lazarus et al. model, since the expansion of the plasma sheet out to L $\sim$25 could prevent the ring material from producing significant concentrated attenuation of the plasma, but rather a modest distributed attenuation. Because of the inward and outward motions of the magnetosphere around local noon caused by changes in solar wind ram pressure, one might not expect the density enhancements to line up there. With the Goertz model, the plasma blobs once formed are expected to be lost down the tail; so one does not expect to see them between midnight and dawn local time. At present, we feel the observations favor the Eviatar et al. and Goertz models which are not necessarily inconsistent with each other, do not require the presence of a distributed source of cold plasma to explain the observations, and are not inconsistent with the expected radial motions of the magnetosphere at these

radial distances ($L \gtrsim 14$). In fact, the model by Eviatar et al. (1982) requires such motion.

Extended Plasma Sheet

The extended plasma sheet appears to be a more stable structure with inner boundary at $L \sim 7$ inside of which a definite reduction in plasma sheet thickness takes place. Densities range between 0.1/cm^3 and 2.0/cm^3, while temperatures range between 100 eV and 20 eV. Along the noon meridian the outer boundary of the extended plasma sheet is at $L \sim 15$; in the midnight-dawn quadrant it terminates at $L \sim 11$ for Voyager 1 at 0330 local time, and extends beyond L=25 for Voyager 2 along the dawn meridian. The outer boundary of the extended plasma sheet in the midnight-dawn quadrant is evidently strongly dependent on external solar wind conditions. It seems plausible that the extended plasma sheet underwent a considerable expansion at the time of the Voyager 2 encounter, when Saturn probably was in Jupiter's tail, and that whole sections of the extended plasma sheet can become detached and lost down Saturn's magnetotail (Behannon et al., 1981; Bridge et al. 1982), similar to the substorm phenomena believed to be taking place at earth (Hones, 1979). Frank et al. (1980) suggested that because of the high plasma β they observed outside L=6, the plasma sheet would be unstable to such phenomena.

Within the extended plasma sheet, outside L=10, the computed scale height for cold O^+ ions ranges between 2 and 4 R_S and the scale heights for the lighter H^+ ions are a factor of 4 larger, ranging from 8 to 16 R_S. Evidently, the flux tubes are completely filled with ionized hydrogen for which the principal containing force is the magnetic mirror force. Hence, it is not surprising to observe a thickness for the extended plasma sheet in excess of 4 R_S.

The extended plasma sheet is a region within which the cold electrons dominate the density $n_H/n_e \sim 15\%$, while almost all the electron pressure is partitioned to the hot suprathermal electrons $P_H/P_e \sim 80\%$. We note that the inner boundary of the extended plasma sheet nearly coincides with the inner boundary of the neutral hydrogen cloud $L \sim 8$, while the large vertical extent

of the extended plasma sheet $H_i > 4\ R_S$ may have some relationship to the large vertical thickness ($8.5\ R_S$) of the neutral hydrogen cloud. The outer boundary of the extended plasma sheet at L~15 near local noon (termination of cold plasma) is probably caused by centrifugal forces (Goertz, 1983). We suggest that the cold plasma comes from the inner plasma torus, which is heated within the extended plasma sheet as it is transported outward by centrifugal forces. The plasma β within the extended plasma sheet is probably ~1.0 where almost all the pressure is contributed by the hot ions. Overall, the ion pressure probably exceeds the electron pressure by more than a factor of 5.

Inner Plasma Torus

The inner plasma torus, with outer boundary at L~7, is a region of reduced scale height $H_i < 1\ R_S$ and of temperatures which may fall below 1 eV at times. Evidence has been presented for a localized reduction in electron temperature near the L shells of Tethys, Dione and possibly Rhea. Analysis difficulties do not allow us to say much about conditions near Enceladus and Mimas.

The electron densities within the inner plasma torus, near the equatorial plane, are considerably greater than in the extended plasma sheet and hot outer magnetosphere. Near the Voyager 1 ring plane crossing ($L \lesssim 6.3$) electron densities are observed to be $\lesssim 40/cm^3$, while during the Voyager 2 ring plane crossing (L~2.88) they probably exceeded $100/cm^3$. Because the plasma sheet is considerably thinner in the inner plasma torus, its plasma content may be less than that in the extended plasma sheet (Bridge et al., 1982). Inside L~6, the plasma beta is estimated to be much less than one, while outside L~6 near the equatorial plane, it may approach 1 (Frank et al., 1980, Krimigis et al., 1983).

Depletion of Hot Electrons

In sections 6 and 7, we presented evidence for the depletion of suprathermal electrons within the inner magnetosphere, which was most dramatic within the inner plasma torus. The first report of this depletion

of hot electrons was given by Sittler et al. (1981). At times, the depletions are observed to be enhanced, over scale lengths ~1 R_S, near the L shells of Tethys, Dione, and Rhea. Whenever these depletions occur, the cold electrons are observed to be cooler, strongly suggesting that the electrons are interacting with neutral material. Inelastic collisions with neutral material will move suprathermals to lower energies, and production of secondary electrons will further populate the cold electron energy states.

Icy Satellites, Diffuse E Ring and Main Rings

Within Saturn's inner magnetosphere there are a number of concentrations of neutral material which can be sources of cold plasma and/or sinks of hot plasma. Saturn's inner icy satellites (Mimas, Enceladus, Tethys, Dione and Rhea) are cold spots in the inner magnetosphere, and the E ring and main ring system are more distributed cold neutral material. The satellites and rings also produce clouds of neutral gas by a number of different mechanisms. Photo-sputtering from the main ring system has been proposed (Carlson, 1980) as the primary source mechanism for the dense (~400/cm^{-3}) hydrogen cloud around Saturn (Weiser et al., 1977; Carlson, 1980; Judge et al., 1980; Broadfoot et al., 1981). Because of the small size and low density of the inner satellites their escape speeds are typically less than 0.5 km/s. This translates to escape energies for water molecules that are a fraction of an electron volt, or equivalently to a thermal energy of 240°K. Since satellite temperatures are typically less than 100°K (Hanel et al., 1981, 1982), sublimation is probably not an important source. But gas emitted by sputtering due to photon and particle impact upon the satellite surfaces may be able to escape and produce concentrations of neutral gas about the orbital positions of the satellites (see Brown et al., 1982). The observed concentration of the E ring particles near the orbital position of Enceladus, argues that Enceladus is the source of the E ring (Terrile and Tokunaga, 1980 and Baum et al., 1980, 1981) and mechanisms similar to that producing Saturn's E ring, could be injecting neutral gas directly into Saturn's magnetosphere. As discussed in Cheng et al. (1982), the lifetime of the E-ring micron sized particles is ~10^4 years/micron, because of

erosion processes produced by particle sputtering and photonsputtering, they must therefore be continually replenished. The satellite Dione also displays some surface structure, indicating resurfacing and the emission of water ice or frost from its fracture system (Smith et al., 1981). Kurth et al. (1981) have suggested that release of volatiles from this fracture system could directly inject neutral gas into the magnetosphere.

In the case of the E ring, Baum and Kreidl (1982) reported ring opacities of $\sim 10^{-6}$ near Enceladus and less than 10^{-8} at L $\sim$8; an abrupt increase in ring brightness occurs inside L $\sim$5. The ring thickness varies from $\lesssim$ 8000 km near Enceladus to greater than 35,000 km at L $\sim$8. Though observed ring opacities are believed to have an accuracy better than 10% in regions where the E ring is optically brightest, the measurements as reported by Baum and Kreidl are not sensitive to dust particles less than 0.2 μm (W. A. Baum, private communication). Therefore, if there are many submicron sized dust particles present, observed ring opacities, which should be thought of as lower estimates, may be significantly larger.

Energy Dependence of Depletions

As discussed in section 7, the general trend for the observed depletion of suprathermal electrons below 6 keV is that the attenuation is greatest at the higher electron energies (bite-out). Whenever the depletions extend below 100 eV, the energy dependence can become more difficult to discern because of instrument sensitivity limitations. When we combine the above information with the energy dependent signatures in the electron fluxes observed by the LECP instrument as reported by Krimigis et al. (1981, 1982, 1983), it becomes evident that electrons are depleted at energies intermediate between the maximum PLS energy electron fluxes are observed above signal threshold (E < 6 keV) and the lower LECP energy channels (E $\lesssim$ 50 keV). For scale lengths $\sim$1 R_S, the depletions move to lower energies with decreasing radial distance.

Interactions with Dust

One can show that this energy dependent signature is consistent with the electrons interacting with micron sized dust particles. The

attenuation of electrons will maximize at energies for which their range through neutral material is approximately equal to the diameter of the dust particles. The breadth in energy of such a bite-out feature will depend upon the size distribution of the dust particles. This comes about because at lower electron energies, at which the electron loses all its energy during a collision, the collision frequency is proportional to the electron speed, since the cross-section for the interaction is simply the cross-sectional area of the dust particle. When the bounce motion of a trapped electron moves it above or below the equatorially confined ring particles, the bounce frequency is proportional to electron speed (Schulz and Lanzerotti, 1974). At higher energies, for which the electron ranges are large compared to dust particle dimensions, the electron loses only a small fraction of its total energy. Therefore, even though these more energetic electrons have more frequent collisions with the dust particles, their fractional energy loss per unit time is less. With these comments in mind, we refer the reader to Figure 2 in Krimigis and Armstrong (1982), where the 22 to 35 keV Voyager 2 electron fluxes display a broad minimum between L=3.5 and L=5.5, while the more energetic E > 1.5 Mev electrons show a steady rise through this region. Though not necessarily a unique signature of ring material, the zone mapped out by this feature nearly coincides with the enhanced portion of the E ring.

In addition to this, the Voyager 2 data displays a strong depletion of suprathermal electrons above 140 eV inside L=5 inbound and outbound. As noted in Sittler et al. (1981), a strong bite-out of the hot electrons occurs near the minimum L shell (L=4.4) approached by the Voyager 1 spacecraft. Therfore, it seems reasonable to suggest that the attenuations inside L=5 are probably caused by the enhanced E ring inside L=5.

Electron Precipitation by Waves

Gurnett et al. (1981) and Scarf et al. (1982) reported the observation of whistler mode emission (chorus and hiss) and electrostatic half-harmonic emissions within Saturn's magnetosphere. Whistler mode turbulence at Saturn is expected to be enhanced near the equatorial plane where the densities are higher and magnetic field a minimum, since the

critical resonance energy $E_{CR}=B^2/(8\pi n_e)$ will be smaller so that more electrons can resonate with the waves there. Whether they will be more important within the inner plasma torus is dependent upon the radial variation of E_{CR}. Between L$\sim$10 and 15 we estimate E_{CR} to be $\sim$500 eV near the equatorial plane. At the Voyager 1 ring plane crossing at L$\sim$6.3 it is probably greater than 600 eV, while during the Voyager 2 ring plane crossing at L$\sim$3 it probably exceeded 10 keV. So, if whistler mode waves are contributing to the depletion of hot electrons below 6 keV, and pressure anisotropies for the hot electrons are not too large ($T_\perp/T_\parallel \sim 2$) they are expected to be most important outside of L$\sim$5.

In the case of electrostatic half-harmonic waves, it is not obvious where most of the pitch angle scattering will occur and whether it will be most important in the inner plasma torus where the suprathermal electrons are most strongly depleted. Depending upon the plasma conditions, these waves will be unstable for either large or small ratios of n_C/n_H (Hubbard and Birmingham, 1978). Narrow band electrostatic waves, which become more unstable near the upper-hybrid resonance frequency f_{UHR} for $n_C/n_H \gg 1$ (Birmingham et al., 1981), are expected to be more unstable near the equatorial plane. Ashour-Abdalla and Kennel (1978), found instability for $n_C/n_H \lesssim 1$ when f_{UHR} was not much larger than the electron gyro-frequency f_g. Here pitch angle scattering will be more effective at higher latitudes, where cold plasma will contribute less to the electron density and $f_g > f_{pc}$ (the cold electron plasma frequency).

If waves are producing the observed depletion of electrons we call bite-outs, then the interaction must be such that they precipitate electrons more effectively at intermediate energy, say 1 keV to 60 keV, than at lower or higher energies. In the case of whistler mode emissions, this implies that the wave turbulence is confined to a band of frequencies. Electrostatic waves which are confined to narrow frequency bands interact with electrons over an intermediate range of electron energies (Lyons, 1974); the waves interact strongly with hot electrons with energies just above $0.5T_H$, such that at higher electron energies the pitch-angle diffusion coefficient decreases with increasing electron energy with a $1/E^{3/2}$ dependence. In addition to the above observational constraint, the

observed depletion of hot electrons is associated with a corresponding cooling of the cold electrons; or alternatively the depletion of hot electrons is associated with the presence of a colder and possibly denser population of cold electrons. Therefore, if waves are producing the depletion of hot electrons, they should behave in such a way that the cold electrons are cooled as the hot electrons become depleted, or are more effective in regions where the cold plasma is colder and possibly more abundant.

The wave amplitudes must also be sufficiently high to cause the strong energy dependent depletion of suprathermal electrons. Recent calculations by Scarf et al. (1983), using plasma wave data obtained during the Voyager 1 ring plane crossing, find the observed whistler mode emissions to be only adequate enough to support weak pitch angle scattering. Kurth et al. (1983) report amplitudes for electrostatic waves during the ring plane crossing which are also too weak to produce any significant precipitation of hot electrons. Since these waves are predominantly confined near the equatorial plane and since the Voyager spacecraft are generally at high magnetic latitudes, significant wave amplitudes could be present near the equatorial plane elsewhere within Saturn's magnetosphere and not be observed (Kurth et al., 1983). Though not overwhelmingly supportive, the current analysis does not necessarily rule out wave-particle interactions as a factor in shaping the observed electron distribution function.

Alternate Possibilities

From the preceding discussion on interactions with dust, one can describe the energy dependence of the electron interaction with dust in terms of an effective collision frequency. This collision frequency will increase with increasing electron energy at low energies, maximize at some intermediate energy (6 keV for 10 micron sized dust particles), and then be a decreasing function of electron energy at higher energies. In many respects the electron impact ionization collision frequencies of neutral gas and plasma ions (i.e., $O^+ + e = O^{++} + 2e$) have a similar energy dependence, except that they peak around 100 eV, above which they decrease monotonically with a $1/E^{1/2}$ dependence. Below 100 eV, electrons at higher

energies will be more effectively depleted (steepening of spectrum), while above 100 eV the electrons will be more effectively removed at lower energies (hardening of spectrum). Therefore, inelastic collisions with neutral gas or plasma ions cannot account for the bite-out signatures observed above a few hundred eV which we associate with dust or plasma waves. They may contribute to some of the observed depletions which extend below 100 eV or the cooling of the cold electrons. Also, ionizing collisions with plasma ions (O^+) will always be taking place, and the observed large scale cooling of electrons will be caused in part by them. But, such effects cannot account for the large number of observed depletions of hot electrons above a few hundred eV, for which the depletions are greater at higher energies.

If there were a direct interaction with a satellite (i.e., no substantial atmosphere or internal magnetic field), plasma dropouts similar to those seen in Jupiter's magnetosphere by Voyager 2 and associated with Ganymede (Burlaga et al., 1980) would be produced, but are not seen here. Often the bite-out signatures are associated with enhancements in density and corresponding reductions in temperature of the cold electrons, consistent with interactions with diffuse clouds of gas, plasma ions, or ring material. We therefore rule out this possibility. An interaction similar to that seen at Titan (Bridge et al., 1981) where the satellite has a relatively dense atmosphere (or exosphere) can also be ruled out with regard to the bite-out signatures above a few hundred eV. In the case of Titan > 700 eV magnetospheric electrons have gyro-radii comparable to or larger than an atmospheric scale height; therefore these electrons with gyrocenters confined outside the ionopause will gyrate deeper into Titan's atmosphere and be preferentially depleted relative to the lower energy electrons (Bridge et al., 1981). Estimated atmospheric scale heights are $\sim$200 km for Dione (assumed H_2O atmosphere with temperature equal to 100°K) while gyro-radii for a 1 keV electron is $\sim$1 km. Since electrons of different energy and thus different gyro-radii will pass through regions of only moderately different atmospheric density (assume presence of ionopause outside of which draping field lines are confined), an interaction of this sort will not produce the bite-out signatures.

Because the frequency for Coulomb collisions is a strongly decreasing function of electron energy ($1/E^{3/2}$), this mechanism has the wrong energy dependence, to explain the depletions of suprathermal electrons, since the depletions below 6 keV tend to be larger at higher electron energies. Given sufficient time, however, Coulomb collisions will tend to populate those energies centered on the breakpoint energy E_B separating the cold and hot components. Qualitatively, this filling in of the spectrum is suggested by the data.

Conclusion about Proposed Mechanisms

In the preceding discussions we have suggested a number of possible causes for the observed depletion of the suprathermal electrons within Saturn's inner magnetosphere. We have emphasized the importance of using the observed energy dependence of the attenuations as a means of discriminating between the different possibilities. The results of this study are summarized in Table 1. A number of possible explanations have been eliminated such as Coulomb collisions or interactions with neutral gas for the bite-out signatures above a few hundred eV. It appears that dust and plasma waves provide the greatest potential for explaining the bite-out signatures for electrons of intermediate energy. But in general most alternatives cannot be eliminated at the present level of investigation. Reported wave amplitudes can only support weak pitch angle scattering of the electrons; but reported E ring opacities, which should be thought of as lower limits, are also not very large. Calculations (not shown here) also indicate that the plasma sheet ions may be competitive with dust particles, with regard to the amplitude of the depletions. Though unknown, satellite atmospheres and neutral gas clouds may also contribute. In order to make further progress, an extensive combined analysis of all particle (PLS, LECP, and CRS) and plasma wave (PWS) data sets is required, along with consideration of the constraints imposed by radial diffusion and measured ring opacities.

Scale Height Effects

In this section we discuss in detail some of the observed variations in electron density which can be attributed to changes in scale

height of the plasma. In many instances the total content of plasma within a unit flux tube can be constant in time even though large changes in electron density are observed.

Voyager 1: Density, Temperature Anti-correlated

Many of the variations in the electron density within the extended plasma sheet can be explained by variations in the density scale height H_i, without recourse to changing the content of plasma within a unit flux tube. In other words, the measurements do not necessarily reflect radial or azimuthal variations in plasma content within a flux tube, as must be occurring in the more time dependent region outside L=15 local noon, where order of magnitude changes in the density are taking place. The density variations observed by Voyager 1 between L=15 and L=10 inbound and displayed in an expanded time scale in Figure 15 are of particular interest, and show an anti-correlation between n_e and T_e.

The total flux tube content for the ith ion, is proportional to (see Bridge et al., 1981)

$$N_i = B_s \int \frac{n_i(L,Z)\,d\ell}{B(L,Z)} \tag{5}$$

where the integral is evaluated along $\vec{B}$ over the volume occupied by the plasma. If one approximates the density dependence with Eq. 2 and uses a dipole field for B(L,Z), Eq. 5 reduces to

$$N_i = n_i(L,0)\sqrt{\pi}\,H_i L^3 \tag{6}$$

If we assume N_i to be a constant, one can solve for $n_i(L,Z)$, which we then substitute into Eq. 2, yielding the following expression for the density

$$n_i(L,Z) = \frac{N_i}{\sqrt{\pi} H_i L^3}\, e^{-(Z/H_i)^2} \tag{7}$$

For $|Z|/H_i \ll 1$, which is the situation for Voyager 1 inbound, Eq. 7 reduces to

$$n_i(L,Z) = \frac{N_i}{\sqrt{\pi} H_i L^3} \qquad (8)$$

where we see that the density and temperature variations will be anti-correlated ($H_i \propto \sqrt{T}$) provided N_i is a constant. Note, that Eq. 7 displays the L^3 dependence derived in Bridge et al. (1981), which was the original motivation for plotting $n_e L^3$. The H_i dependence in Eq. 7 can modify this L^3 dependence, if H_i is a function of L. The Voyager data shows that $H_i \propto L^m$, where $m > 0$; therefore if m were equal to 1 and if $|Z|/H_i \ll 1$, the density would display $1/L^4$ dependence. Furthermore, if the plasma sheet is very thick, as it is for the light ions H^+, the density n_e will be proportional to $1/L^4$; this might account for the $1/L^4$ dependence indicated by the Voyager 2 data, where the composition is predominantly H^+, Lazarus and McNutt (1983).

The Voyager 1 data show that $|Z|/H_i$, between L=15 and L=10 inbound, satisfies the condition $(Z/H_i)^2 \ll 1$, so that Eq. 8 represents a good approximation for the density dependence upon H_i. Focusing our attention on the boundaries (see Figure 15), at which abrupt density changes occur, we note that the product $n_e H_i$ has a reduced variability across these boundaries (assume composition dominated by heavy ions). Therefore, many of the changes in n_e can be caused by a change in scale height while the total flux tube content N_i remains nearly a constant throughout this region.

Voyager 2: Density, Temperature Correlated

The density and temperature are highly variable within the plasma sheet from L=12 to L=5 inbound, and this variability can mostly be attributed to scale height variations. The variation of n_e and T_e, contrary to that seen by Voyager 1, are positively correlated as shown in Figure 16 with the density enhancements associated with the appearance of cold heavy ions. By increasing their temperature, the scale height for the heavy ions increases, so that they move up to the spacecraft, which is far off the equatorial plane, $|Z|/Hi \gtrsim 1$. Equation 7 is thus dominated by the exponential term; under these circumstances, one expects a positive

correlation between the density and temperature. Model calculations show that the observed variations are consistent with this interpretation, where the total flux tube content is approximately a constant within the extended plasma sheet, independent of radial distance and azimuthal angle.

Since many of the density variations observed within the extended plasma sheet could be attributed to changes in scale height and not total flux tube content, the same situation probably occurs within the inner plasma torus. As noted above and in the main text, the satellites Tethys, Dione, and possibly Rhea are associated with regions of locally cold plasma. This reduction in temperature creates a region of reduced scale height centered on the satellite L shells. Therefore, assuming constant flux tube content (assume satellite not a source of cold plasma, just a cooler of the plasma), the density will maximize at the satellite L shells as one moves in L near the equatorial plane (i.e., the observed profile in Frank et al., 1980). It may be that the reductions in electron temperature are produced by the addition of cold plasma, as seems to be the case for Tethys, which would suggest the satellites are an important source of cold plasma. Therefore, until detailed scale height model calculations making use of the combined results of the ion and electron analysis are completed, one should reserve judgment as to whether or not the satellites Tethys and Dione are significant sources of cold plasma.

Plasma Wave Observations

Comparing observed fluxes of suprathermal electrons and whistler mode emissions reported by Gurnett et al. (1981) we reported evidence for an association between the detection of whistler mode waves and the observed presence of suprathermal electrons. As the suprathermals became hotter and more abundant, the whistler mode emission became broader in frequency and greater in amplitude. When this comparison was done with the Voyager 2 wave data reported by Scarf et al. (1982), the reported whistler mode emissions were evidently in resonance with more energetic electrons; electron fluxes above 140 eV were below signal threshold and resonance energies were considerably higher than that estimated for the Voyager 1 data.

Ring Current

In section 9, we investigated the implications of the plasma data for the ring current model calculations. We compared the electron observations with nearly time coincident ion spectra that have been analyzed, and noted the association suggested by the data betwen the cold (hot) ions and cold (hot) electrons. We suggested that the ion pressure probably exceeds, in general, the electron pressure by more than a factor of 5. From this information, we estimated current densities comparable to those estimated in the model calculations by Connerney et al. (1981). Similar calculations using tne ion data are made in Lazarus and McNutt (1983). As a result of comparisons between model calculations of Connerney et al. and Voyager 1 magnetic field data inside L $\sim$ 8 inbound, and considering that between L=6 and L=8 the plasma beta are $\lesssim$ 1 (Frank et al., 1980; Krimigis et al., 1983), and the Alfvén Mach number is $\lesssim$ 1 (Lazarus and McNutt, 1983), we suggest that better agreement with the magnetometer data could be obtained by a ring current between L=6 and L=8, such that during the Voyager 1 inbound pass the ring current was thinner than that outside L=8. Differences between predictions of model calculations, based on the Voyager 1 data set, with the Voyager 2 outbound magnetic field measurements (Ness et al., 1982), appear to be due to the larger radial extent of the extended plasma sheet observed during the Voyager 2 outbound pass.

Acknowledgments

We thank H. S. Bridge, Head of the Center for Space Research at MIT and Principal Investigator of the Voyager Plasma Science Experiment, for his past and present efforts, support, and advice. His scientific and technical leadership and hard work over many years have made the plasma experiment on Voyager a major success. We extend our appreciation to our other colleagues at MIT (J. W. Belcher, A. J. Lazarus and R. L. McNutt) for their assistance by making available to us results of their ion analysis before publication, and for many useful discussions about the data and its interpretation. We thank N. F. Ness and the Voyager magnetometer team

(NASA/GSFC) for providing to us the magnetic field data used in this report. J. E. P. Connerney (NASA/GSFC) kindly provided predicted times, based on his model calculations, when the Voyager spacecraft were magnetically connected to the equatorial positions of the inner satellites. We also thank the referees for their constructive comments. We are thankful for the data support services provided by P. Harrison, P. Hodge, L. Moriarty and F. Ottens from the data analysis team headed by W. Mish (NASA/GSFC). The drafting support by F. Hunsaker and L. White (NASA/GSFC) is appreciated. Finally, we thank B. Newton (NASA/GSFC) for the many hours spent in typing the manuscript.

TABLE 1. Depletion Mechanisms Summarized

Mechanism	Energy Dependence	L Dependence	Likelihood
Dust	Intermediate Peaks near 6 keV	3.5 - 5.0	Yes
		5.0 - 8.0	Questionable
Whistler Mode	Intermediate if turbulence confined to band of frequencies	$\gtrsim$ 5.0	Yes
		< 5	No
Electrostatic	Intermediate such that $E > 0.5\ T_H$ with $1/E^{3/2}$ dependence at high energies	?	Yes
Neutral Gas Clouds and Plasma Ions	Intermediate Peaks near 100 eV with $1/E^{1/2}$ dependence at higher energies	L > 6 ± 1	No
		L < 6 ± 1	Maybe
Satellite Sweeping			
No atmosphere and magnetic field	All energies†	L < 9	No
With atmosphere and no magnetic field	Intermediate Peaks near 100 eV with $1/E^{1/2}$ dependence at higher energies†	L > 6 ± 1	No
		L < 6 ± 1	Maybe
Coulomb Collisions	$1/E^{3/2}$ dependence	All L	No

†At very high energies E > 10 MeV (for Dione) gyro-radii effects may modify energy dependence.

References

Ashour-Abdalla, M. and C. K. Kennel, Nonconvective and convective electron cyclotron harmonic instabilities, J. Geophys. Res., 83, 1531, 1978.

Baum, W. A., T. Kreidl, J. A. Westphal, G. E. Danielson, P. K. Seidelmann, D. Pascu, and D. G. Currie, Bull. Amer. Astron. Soc., 12, 700-701, 1980.

Baum, W. A., T. Kreidl, J. A. Westphal, G. E. Danielson, P. K. Seidelmann, D. Pascu, and D. G. Currie, Saturn's E ring, Icarus, 47, 84, 1981.

Baum, W. A. and T. J. Kreidl, IAU Colloquium No. 75, "Planetary Rings", Toulouse, France, in press, 1982.

Behannon, K. W., J. E. P. Connerney, and N. F. Ness, Saturn's magnetic tail: Structure and dynamics, Nature, 292, 753, 1981.

Birmingham, T. J., J. K. Alexander, M. D. Desch, R. F. Hubbard, and B. M. Pedersen, Observations of electron gyroharmonic waves and the structure of the Io torus, J. Geophys. Res., 86, 8497, 1981.

Bridge, H. S., J. W. Belcher, A. J. Lazarus, S. Olbert, J. D. Sullivan, F. Bagenal, P. R. Gazis, R. E. Hartle, K. W. Ogilvie, J. D. Scudder, E. C. Sittler, A. Eviatar, G. L. Siscoe, C. K. Goertz, and V. M. Vasyliunas, Plasma observations near Saturn: Initial results from Voyager 1, Science, 212, 217, 1981.

Bridge, H. S., F. Bagenal, J. W. Belcher, A. J. Lazarus, R. L. McNutt, J. D. Sullivan, P. R. Gazis, R. E. Hartle, K. W. Ogilvie, J. D. Scudder, E. C. Sittler, A. Eviatar, G. L. Siscoe, C. K. Goertz, and V. M. Vasyliunas, Plasma observations near Saturn: Initial results from Voyager 2, Science, 215, 563, 1982.

Bridge, H. S., J. W. Belcher, R. J. Butler, A. J. Lazarus, A. M. Mavretic, J. D. Sullivan, G. L. Siscoe, and V. M. Vasyliunas, The plasma experiment on the 1977 Voyager mission, Space Sci. Rev., 21, 259, 1977.

Broadfoot, A. L., B. R. Sandel, D. E. Shemansky, J. B. Holberg, G. R. Smith, D. F. Strobel, J. C. McConnell, S. Kumor, D. M. Hunten, S. K. Atreya, T. M. Donahue, H. W. Moos, J. L. Bertaux, J. E. Blamont, R. B. Pomphrey, and S. Linick, Extreme ultraviolet observations from Voyager 1 encounter with Saturn, Science, 212, 206, 1981.

Brown, W. L., L. J. Lanzerotti, and R E. Johnson, Fast ion bombardment of ices and its astrophysical implications, Science, 218 525, 1982.

Burlaga, L. F., J. W. Belcher, and N. F. Ness, Disturbances observed near Ganymede by Voyager 2, Geophys. Res. Lett., 7, 21, 1980.

Burlaga, L. F., R. Schwenn, and H. Rosenbauer, Dynamical evolution of interplanetary magnetic fields and flows between 0.3 AU and 8.5 AU: Entrainment, submitted to Geophys. Res. Lett., 1983.

Burlaga, L. F., Corotating pressure waves without streams in the solar wind, submitted to J. Geophys. Res., 1983.

Carlson, R. W., Photo-sputtering of ice and hydrogen around Saturn's rings, Nature, 283, 461, 1980.

Cheng, A. F., L. J. Lanzerotti, and V. Pirronello, Charged particle sputtering of ice surfaces in Saturn's magnetosphere, J. Geophys. Res., 87, 4567, 1982.

Connerney, J. E. P., M. H. Acuña, and N. F. Ness, Saturn's ring current and inner magnetosphere, Nature, 292, 724, 1981.

Connerney, J. E. P., N. F. Ness, and M. H. Acuña, Zonal harmonic model of Saturn's magnetic field from Voyager 1 and 2 observations, Nature, 2[illegible] 44, 1982.

Desch, M., Radio emission signature of Saturn immersions in Jupiter's magnetic tail, J. Geophys. Res., in press, 1983.

Eviatar, A., G. L. Siscoe, J. D. Scudder, E. C. Sittler, Jr., and J. D. Sullivan, The plumes of Titan, J. Geophys. Res., 87, 8091, 1982.

Eviatar, A., R. L. McNutt, Jr., G. L. Siscoe, and J. D. Sullivan, Heavy ions in the outer Kronian magnetosphere, J. Geophys. Res., 823, 88, 1983.

Frank, L. A., B. G. Burek, K. L. Ackerson, J. H. Wolfe, and J. D. Mihalov, Plasmas in Saturn's magnetosphere, J. Geophys. Res., 85, 5695, 1980.

Gledhill, J. A., Magnetosphere of Jupiter, Nature, 214, 155, 1967.

Goertz, C. K., Detached plasma in Saturn's turbulence layer, Geophys. Res. Lett., 10, 455, 1983.

Gurnett, D. A., W. S. Kurth, and F. L. Scarf, Plasma waves near Saturn: Initial results from Voyager 1, Science, 212, 235, 1981.

Hanel, R., B. Conrath, F. M. Flasar, V. Kunde, W. Maguire, J. Pearl, J. Pirraglia, R. Samuelson, L. Herath, M. Allison, D. Cruikshank, D. Gautier, P. Gierasch, L. Horn, R. Koppony, and C. Ponnamperuma, Infrared observations of the Saturnian system from Voyager 1, Science, 212, 192, 1981.

Hanel, R., B. Conrath, F. M. Flasar, V. Kunde, W. Maguire, J. Pearl, J. Pirraglia, R. Samuelson, D. Cruikshank, D. Gautier, P. Gierasch, L. Horn, and C. Ponnamperuma, Infrared observations of the Saturnian system from Voyager 2, Science, 215, 544, 1982.

Hartle, R. E., E. C. Sittler, Jr., K. W. Ogilvie, J. D. Scudder, A. J. Lazarus, and S. K. Atreya, Titan's ion exosphere observed from Voyager 1, J. Geophys. Res., 87, 1383, 1982.

Hill, T. W., A. J. Dessler, and F. C. Michel, Configuration of the Jovian magnetosphere, Geophys. Res. Lett., 1, 3, 1974.

Hones, E. W., Jr., Transient phenomena in the magnetotail and their relation to substorms, Space Science Reviews, 23, 393, 1979.

Hubbard, R. F. and T. J. Birmingham, Electrostatic emissions between electron gyroharmonics in the outer magnetosphere, J. Geophys. Res., 83, 4837, 1978.

Judge, D. L., F. M. Wu, and R. W. Carlson, Ultraviolet photometer observations of the Saturnian system, Science, 207, 431, 1980.

Kaiser, M. L., M. D. Desch, J. W. Warwick, and J. B. Pearce, Voyager detection of nonthermal radio emission from Saturn, Science, 209, 1238, 1980.

Kennel, C. F. and H. E. Petschek, Limit on stably trapped particle fluxes, J. Geophys. Res., 71, 1, 1966.

Krimigis, S. M., T. P. Armstrong, W. I. Axford, C. O. Bostrom, G. Gloeckler, E. P. Keath, L. J. Lanzerotti, J. F. Carbary, D. C. Hamilton, and E. C. Roelof, Low-energy charged particles in Saturn's magnetosphere: Results from Voyager 1, Science, 212, 225, 1981.

Krimigis, S. M., T. P. Armstrong, W. I. Axford, C. O. Bostrom, C. Gloeckler, E. P. Keath, L. J. Lanzerotti, J. F. Carbary, D. C. Hamilton, and E. C. Roelof, Low-energy hot plasma and particles in Saturn's magnetosphere, Science, 215, 571, 1982.

Krimigis, S. M. and T. P. Armstrong, Two-component proton spectra in the inner Saturnian magnetosphere, Geophys. Res. Lett., 9, 1143, 1982.

Krimigis, S. M., J. F. Carbary, E. P. Keath, T. P. Armstrong, L. J. Lanzerotti, and G. Gloeckler, General characteristics of hot plasma and energetic particles in the Saturnian magnetosphere: Results from the Voyager spacecraft, J. Geophys. Res., this issue, 1983.

Kurth, W. S., D. A. Gurnett, F. L. Scarf, R. L. Poynter, and J. D. Sullivan, Voyager observations of Jupiter's distant magnetotail, J. Geophys. Res., 86, 8402, 1981a.

Kurth, W. S., D. A. Gurnett, and F. L. Scarf, Control of Saturn's kilometric radiation by Dione, Nature, 292, 742, 1981b.

Kurth, W. S., J. D. Sullivan, D. A. Gurnett, F. L. Scarf, H. S. Bridge, and E. C. Sittler, Jr., Observations of Jupiter's distant magnetotail and wake, J. Geophys. Res., 87, 10373, 1982.

Kurth, W. S., D. D. Barbosa, D. A. Gurnett, and F. L. Kurth, W. S., F. L. Scarf, D. A. Gurnett, and D. D. Barbosa, A survey of electrostatic waves in Saturn's magnetosphere, J. Geophys. Res., this issue, 1983.

Lazarus, A. J. and P. R. Gazis, The radial evolution of the solar wind, 1-10 AU, Solar Wind 5 Proceedings, ed. M. Neugebauer, in press, 1983.

Lazarus, A. J., T. Hasegawa, and F. Bagenal, Long-lived particulate or gaseous structure in Saturn's outer magnetosphere?, Geophys. Res. Lett., in press, 1983.

Lazarus, A. J. and R. L. McNutt, Jr., Low energy plasma ion observations in Saturn's magnetosphere, J. Geophys. Res., this issue, 1983.

Lepping, R. P., L. F. Burlaga, M. D. Desch, and L. W. Klein, Evidence for a distant (> 8700 R_J) Jovian magnetotail: Voyager 2 observations, Geophys. Res. Lett., 9, 885, 1982.

Lepping, R. P., M. D. Desch, L. W. Klein, E. C. Sittler, Jr., J. D. Sullivan, W. S. Kurth, and K. W. Behannon, Structure and other properties of Jupiter's distant magnetotail, J. Geophys. Res., this issue, 1983.

Lyons, L. R., Electron diffusion driven by magnetospheric electrostatic waves, J. Geophys. Res., 79, 575, 1974.

Ness, N. F., M. H. Acuña, R. P. Lepping, J. E. P. Connerney, K. W. Behannon, L. F. Burlaga, and F. M. Neubauer, Magnetic field studies by Voyager 1: Preliminary results at Saturn, Science, 212, 211, 1981.

Ness, N. F., M. H. Acuña, K. W. Behannon, L. F. Burlaga, J. E. P. Connerney, R. P. Lepping, and F. M. Neubauer, Magnetic field studies by Voyager 2: Preliminary results at Saturn, Science, 215, 558, 1982.

Rossi, B. and S. Olbert, Introduction to the physics of space, McGraw-Hill, 1970.

Sandel, B. R., D. E. Shemansky, A. L. Broadfoot, J. B. Holberg, G. R. Smith, J. C. McConnell, D. F. Strobel, S. K. Atreya, T. M. Donahue, H. W. Moos, D. M. Hunten, R. B. Pomphrey, and S. Linick, Extreme ultraviolet observations from the Voyager 2 encounter with Saturn, Science, 215, 548, 1982.

Scarf, F. L., W. S. Kurth, D. A. Gurnett, H. S. Bridge, and J. D. Sullivan, Jupiter tail phenomena upstream from Saturn, Nature, 292, 585, 1981.

Scarf, F. L., D. A. Gurnett, W. S. Kurth, and R. L. Poynter, Voyager 2 plasma wave observations at Saturn, Science, 215, 587, 1982.

Scarf, F. L., D. A. Gurnett, W. S. Kurth, and R. L. Poynter, Voyager plasma wave measurements at Saturn, J. Geophys. Res., this issue, 1983.

Schulz, M. and L. J. Lanzerotti, Particle diffusion in the radiation belts, Springer, New York, 1974.

Scudder, J. D., E. C. Sittler, Jr., and H. S. Bridge, A survey of the plasma electron environment of Jupiter: A view from Voyager, J. Geophys. Res., 86, 8157, 1981.

Sittler, E. C., Jr., J. D. Scudder, and H. S. Bridge, Detection of the distribution of neutral gas and dust in the vicinity of Saturn, Nature, 292, 711, 1981.

Sittler, E. C., Jr., Plasma electron analysis: Voyager Plasma Science Experiment, NASA TM 85037, 1983.

Smith, E. J., L. Davis, Jr., D. E. Jones, P. J. Coleman, Jr., D. S. Colburn, P. Dyal, and C. P. Sonett, Saturn's magnetosphere and its interaction with the solar wind, J. Geophys. Res., 85, 5655, 1980.

Smith, B. A., L. Soderblom, J. Boyce, G. Briggs, A. Bunker, S. A. Collins, C. J. Hansen, T. V. Johnson, J. L. Mitchell, R. J. Terrile, M. Carr, A. F. Cook, II, J. Cuzzi, J. B. Pollack, G. E. Danielson, A. Ingersoll, M. E. Davies, G. E. Hunt, H. Musursky, E. Shoemaker, D. Morrison, T. Owen, C. Sagan, J. Veverka, R. Strom, and V. E. Suomi, Encounter with Saturn: Voyager 1 imaging science results, Science, 212, 163, 1981.

Strobel, D. F. and D. E. Shemansky, EUV emission from Titan's upper atmosphere: Voyager 1 encounter, J. Geophys. Res., 87, 1361, 1982.

Terrile, R. J. and A. Tokunaga, Infrared photometry of Saturn's E-ring, Bull. Am. Astr. Soc., 12, 701, 1980.

Weiser, H., R. C. Vitz, H. W. Moss, Detection of Lyman α emission from the Saturnian disk and from the ring system, Science, 197, 755, 1977.

Wolfe, J. H., J. D. Mihalov, H. R. Collard, D. D. McKibbin, L. A. Frank, and D. S. Intriligator, Preliminary results on the plasma environment of Saturn from the Pioneer 11 plasma analyzer experiment, Science, 207, 403, 1980.

Wu, C. S. and R. C. Davidson, Electromagnetic instabilities produced by neutral-particle ionization in interplanetary space, J. Geophys. Res., 77, 5399, 1972.

FIGURE CAPTIONS

Figure 1a — Trajectories of the Pioneer 11, Voyager 1 and Voyager 2 spacecraft projected onto Saturn's equatorial plane. The coordinate system is Saturn centered with the X axis pointing along the Saturn-Sun line, and the Y axis completes the right-handed coordinate system where the Z axis is aligned along Saturn's spin axis. Average modeled bow shock and magnetospause boundaries from Bridge et al. (1982) have been superimposed upon the figure. Observed bow shock (S) and magnetopause crossing positions from Wolfe et al. (1980) for Pioneer 11 and Bridge et al. (1981, 1982) for Voyager 1 and 2, respectively, have been projected onto the equatorial plane. All distances are in units of Saturn radius R_S = 60,330 km.

Figure 1b — Meridional view of the Pioneer 11, Voyager 1 and Voyager 2 trajectories in the same Saturn-centered coordinate system defined for Figure 1. The abscissa is the equatorial radial distance R and the ordinate is the Z axis which is aligned along Saturn's spin axis. Dipole field lines have been added for reference purposes.

Figure 2 — Colored illustration of Saturn's magnetosphere as defined by the plasma electrons. On the left, we have a composite view of the Voyager 1 and 2 inbound observations near the noon meridian. The right-hand view is more characteristic of the outbound observations within the dawn-midnight quadrant. Cold regions are colored blue, regions of intermediate temperature are purple (blue plus red), and the hot regions are red. The cold thermal electrons are predominantly confined within the bluer region near the equatorial plane, whose vertical extent is equal to the locally estimated scale height of the cold heavy ions (see text). The hotter suprathermal electrons are defined by the redder regions at higher latitudes and larger radial

distances which are confined outside the outer radial boundary of the extended plasma sheet. Note that cold electrons will also reside at higher latitudes because of light ions (but at a reduced number density relative to that within the bluer regions) and the hot electrons will also reside within the bluer regions at lower latitudes. This technique of separating cold and hot regions has only been done for illustration purposes. This figure is neither a density nor temperature distribution map. The gradations in temperature indicated by color change pertain to each individual region--cold electron component (blue region) and hot electron component (red region).

The three major plasma regions: hot outer magnetosphere, extended plasma sheet, and inner plasma torus are denoted. For reference purposes, the satellite positions (M, E, T, D, and R for Mimas, Enceladus, Tethys, Dione and Rhea, respectively), E ring (gray shaded rectangular region), neutral hydrogen cloud (circular region with white dots), and magnetopause boundary are displayed. The gray backing for the neutral hydrogen cloud has been added to allow visibility of the white dots. The E ring opacity is illustrated by a gray shading scheme, such that regions of greater opacity are darker. The field line topology is drawn to conform to that given in Connerney et al. (1981) which includes the effects of Saturn's ring current. Titan plumes and detached plasma "blobs" as described in Eviatar et al. (1982) and Goertz (1983), respectively, are displayed in the noon meridian view. On the right, we have suggested the possibility of some stretching of the field lines near the equatorial plane. Finally, the white regions within the magnetosphere signify regions for which we have no information.

Figure 2 (Black and White Caption)

This figure is a black and white version of the colored figure. See colored figure with caption for description.

Figure 3 Voyager 1 moment electron density (n_e), moment electron temperature (T_e), cold ion scale height H_i(O^+ ion left-hand scale (H_{O+}); H^+ ion right-hand scale (H_{H^+})), and ratio of spacecraft distance from equatorial plane |Z| over ion scale height H_i (O^+ ions left-hand scale; H^+ ions right-hand scale) plotted versus dipole L shell. In the top panel Saturn-Sun and Ring-Sun UV occultation regions are denoted; in these regions the spacecraft may have a negative potential and if so, the density and temperature will be underestimated and overestimated, respectively. Magnetopause (MP), Titan flyby, and sample spectra positions are indicated. In the panel next from the top, the inner satellite positions computed according to the Connerney et al. (1981, 1982) magnetic field model calculations are denoted. In the lower panel, the regions where the heavy, light cold ions are expected to dominate the cold ion composition are indicated.

Figure 4 Same as Figure 3, except Voyager 2 parameter estimates are plotted versus dipole L. The data analysis is uncertain within intervals A and B and should be interpreted with caution; see text for details.

Figure 5 Figure shows gradual disappearance of cold electron component as the Voyager 2 spacecraft approaches Saturn inside Dione's L shell, Each panel is a plot of the reduced electron distribution function F_e (as defined in Sittler, 1983) versus electron speed. Cne telemetry cound and instrument noise levels are indicated. The breakpoint energy E_B is denoted.

Figure 6 Time plot of Voyager 2 electron density and temperature estimates near the outer boundary of the extended plasma sheet in the noon sector. The total electron density (n_e) and temperature (T_e) and cold electron density (n_c) and temperature (T_c) are displayed. The figure clearly demonstrates the order of magnitude change in density and temperature in the hot outer magnetosphere and the anti-correlation between n_e and T_e.

Figure 7 Voyager 1 electron speed distributions f_e measured at the outer boundary of the extended plasma sheet near the noon meridian (position 1 in Figure 3). Spectra measured only 192 seconds apart, show the rapid variability in density of cold plasma. One telemetry count and instrument noise levels are indicated. For reference, the electron energy in eV is indicated at the top of panel. Along the abscissa is the electron speed v_d outside the photoelectron sheath surrounding the spacecraft. Dashed lines indicate Maxwellian fit to cold component. The hot density n_H and hot temperature T_H were computed by setting $n_H = n_e - n_c$ and $T_H = (n_e T_e - n_c T_c)/n_H$. This method is different from that used to produce profiles in Figure 11 (see Sittler, 1983).

Figure 8 Voyager 2 electron speed distributions measured within the hot outer magnetosphere near local noon (position 2 in Figure 4). Here spectra are only 96 seconds apart. Same format used in Figure 7 is used here.

Figure 9 Voyager 1 electron speed distribution measured within the extended plasma sheet near noon local time (positions numbered 3 and 4 in Figure 3). Same format used in Figure 7 used here. Note that all signal for the spectrum measured at 1834:06 is below instrument threshold (one TMC level) for speeds above 20,000 km/s.

Figure 10 Same as Figure 9, except Voyager 2 electron speed distributions are plotted. They are located at positions numbered 5 and 6 in Figure 4.

Figure 11 Five minute averages of the fractional density n_H/n_e and fractional pressure P_H/P_e partitioned to the suprathermal electrons are plotted versus dipole L for Voyager 1 (top 2 panels) and Voyager 2 (bottom 2 panels). See Sittler (1983) for definitions. The data analysis is uncertain within intervals A and B for Voyager 2 and should be interpreted with caution; see text for details.

Figure 12 Time plot of Voyager 1 3.2 minute averages of electron flux density integrated over the energy band from 280 eV to 5950 eV. This figure displays the observed time variation of suprathermal electron fluxes. Periods beginning and ending with X symbols are intervals within which signal is less than 6 times instrument noise, very near instrument signal threshold. The gaps without X symbols bracketing them are data gaps. Therefore, the period from ~ 19:30 to ~ 21:30 only contains signal near instrument noise and signal threshold for energies between 280 eV and 5950 eV. The satellite L shell crossing times based on the Connerney et al. (1981, 1982) predictions are indicated. Intervals A and B indicate periods when LECP stepping was at a 6 second rate. Flux levels are probably higher within the B interval, during which time the data displays the presence of interference in the higher energy channels.

Figure 13 The electron pressure P_e and electron beta β_e plotted versus dipole L for Voyager 1 (top 2 panels) and Voyager 2 (bottom 2 panels). Magnetic field strength supplied courtesy N. F. Ness principal investigator of the Voyager magnetometer team.

Figure 14 Electron speed distribution measured during the Voyager 1 outbound ring plane crossing period (position 7 in Figure 3). Measured nearly time coincident with the ion spectrum in Figure 17 in Lazarus and McNutt (1983). Same format used in Figure 7 used here.

Figure 15 Time plot of Voyager 1 electron density and temperature within the extended plasma sheet near local noon. Same format used in Figure 6 is used here. Figure shows a definite anti-correlation between n_e and T_e, which could be caused by changes in plasma sheet thickness and not total flux tube content.

Figure 16 Time plot of Voyager 2 electron density and temperature near the boundary separating the extended plasma sheet and inner plasma torus (inbound data). Same format used in Figure 6 is used here. Figure shows positive correlation between n_e and T_e, which can be shown to be caused by changes in plasma sheet thickness (total flux tube content is constant).

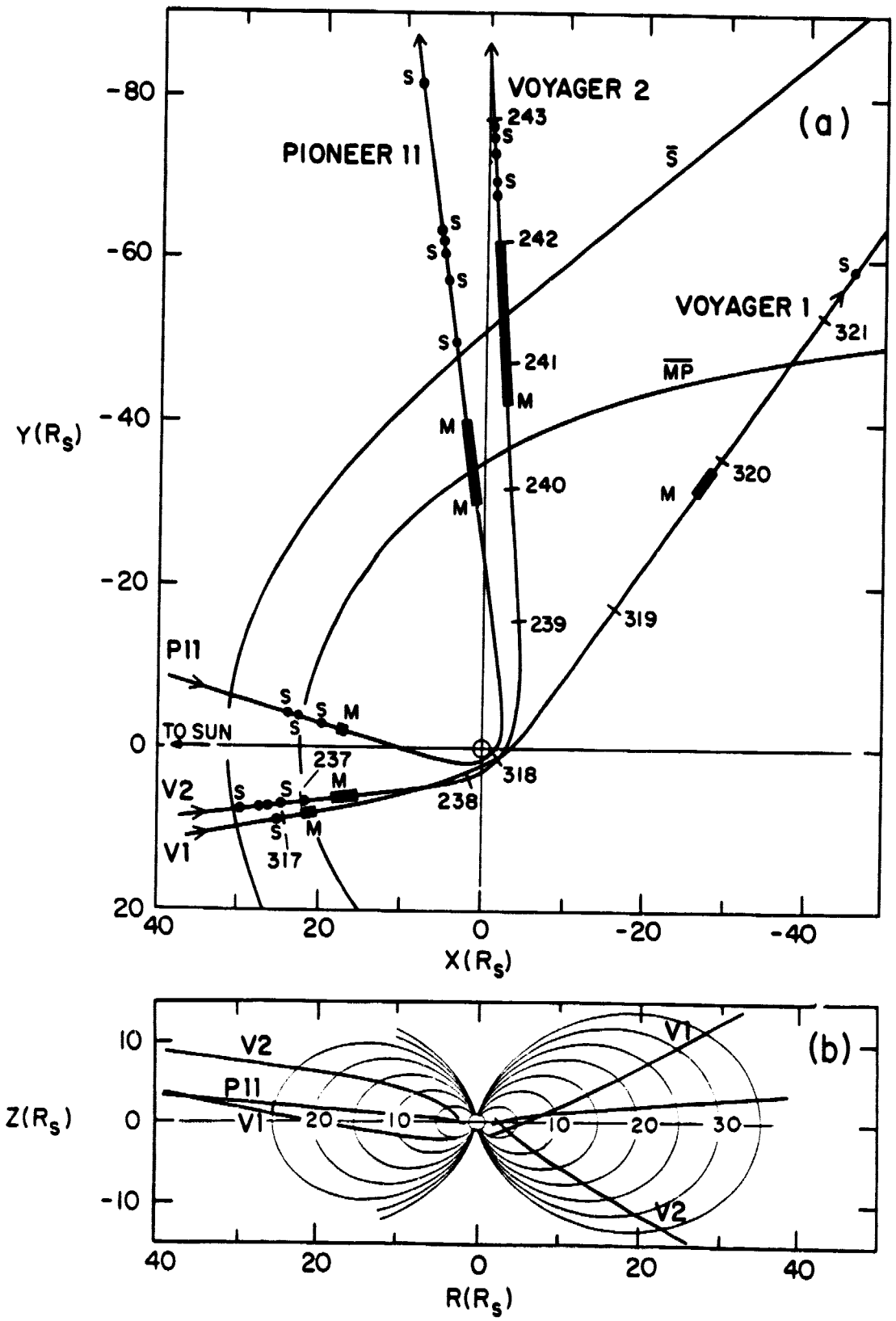

Figure 1

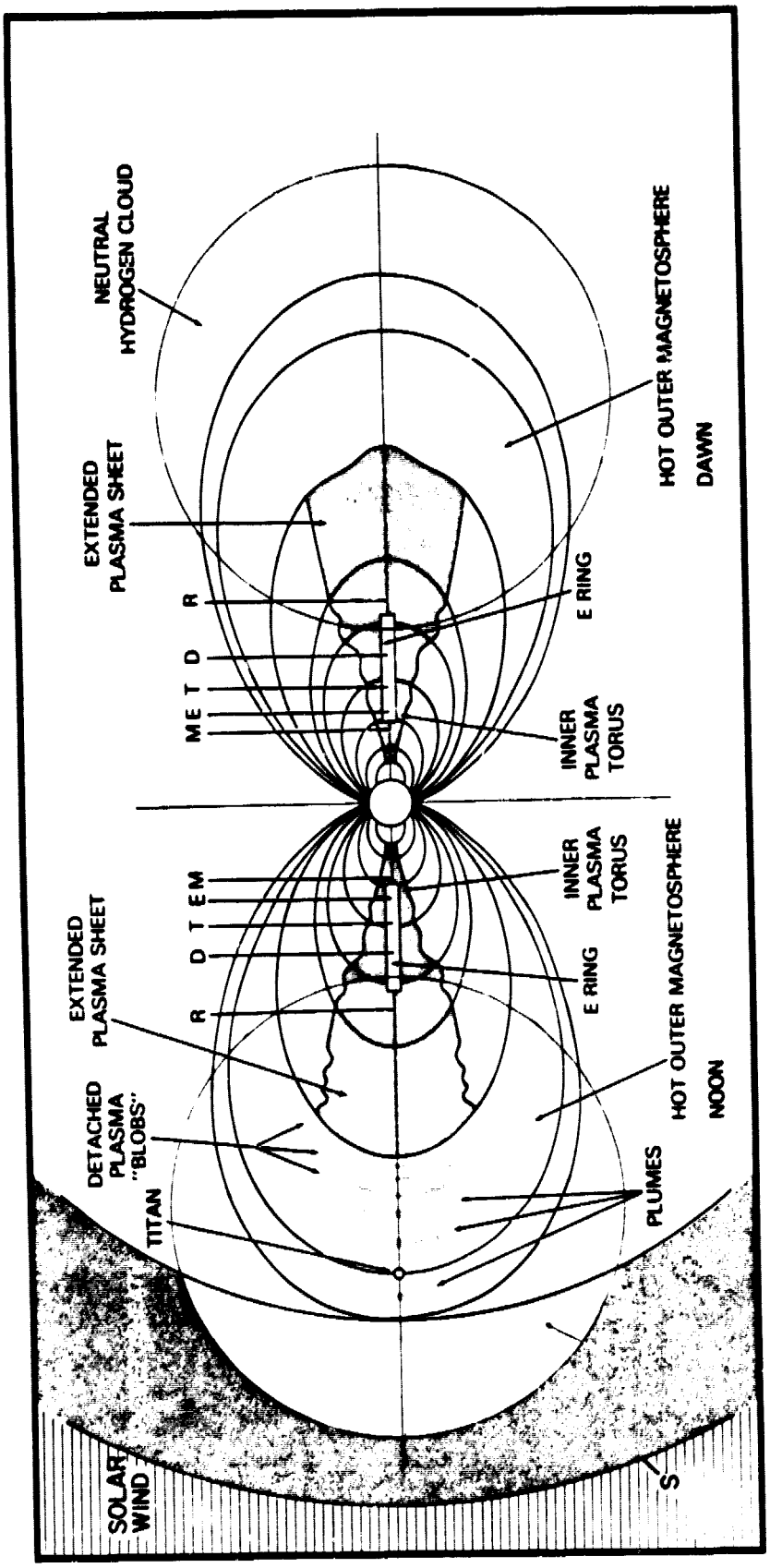

Figure 2

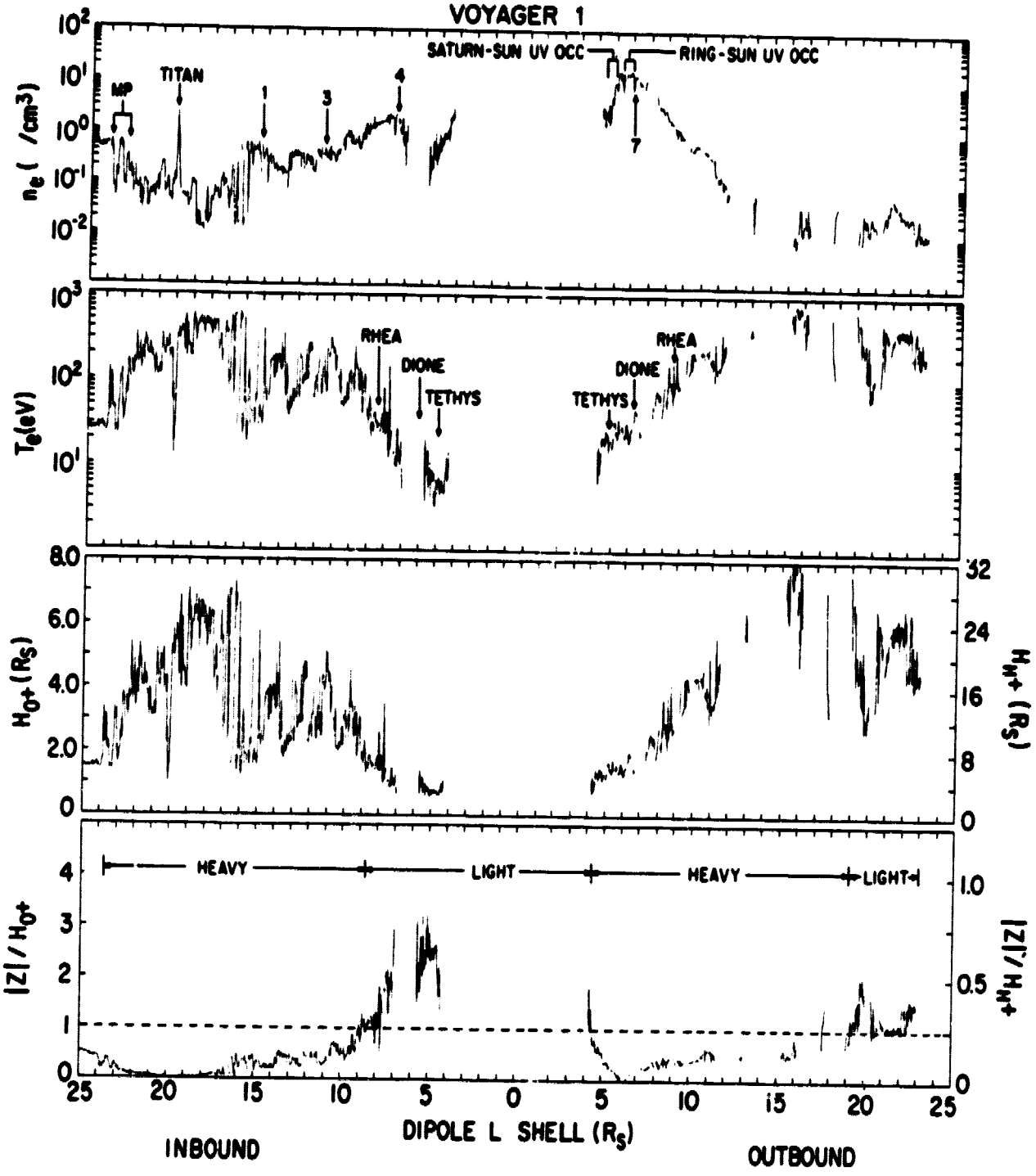

Figure 3

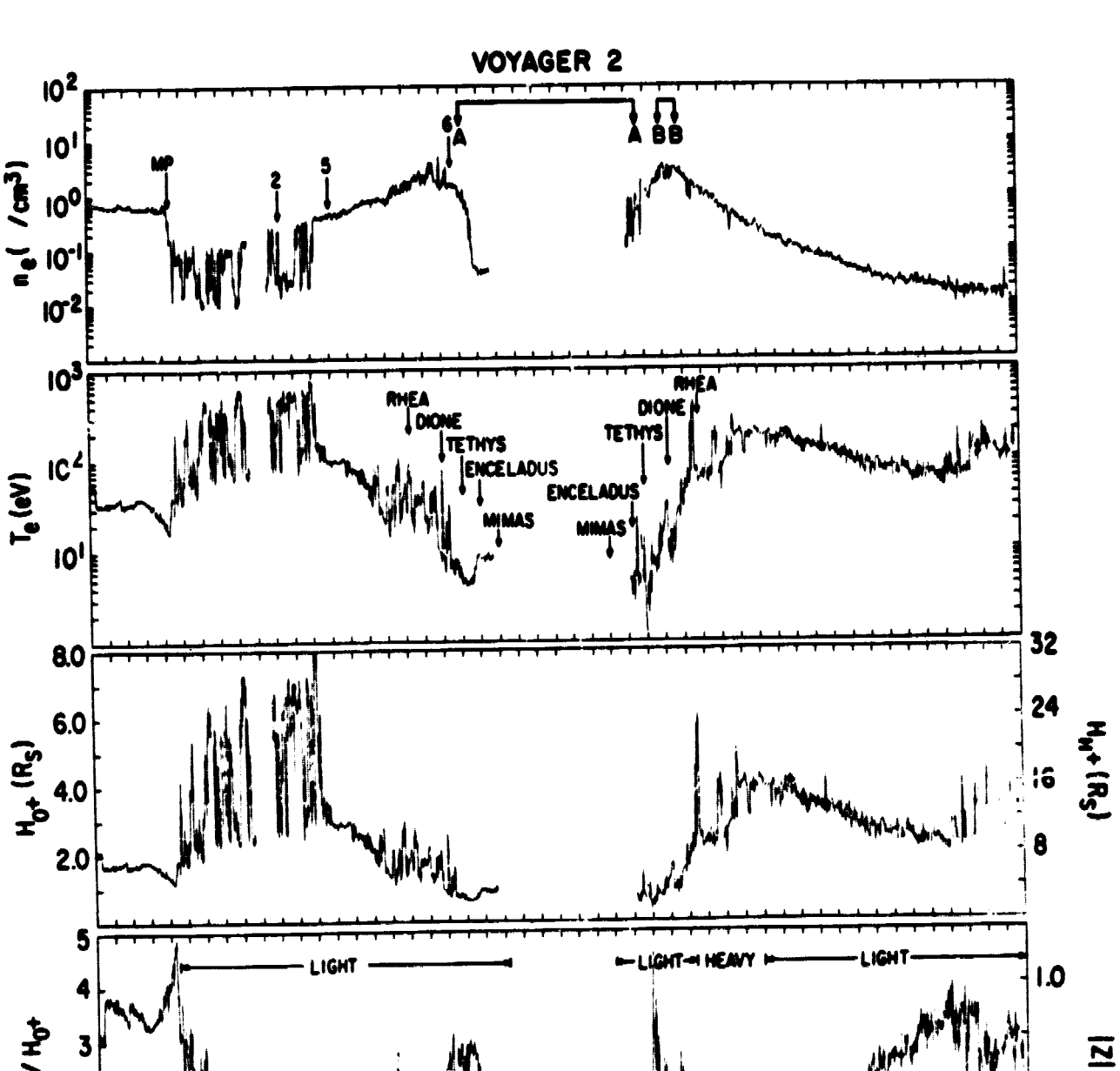

Figure 4

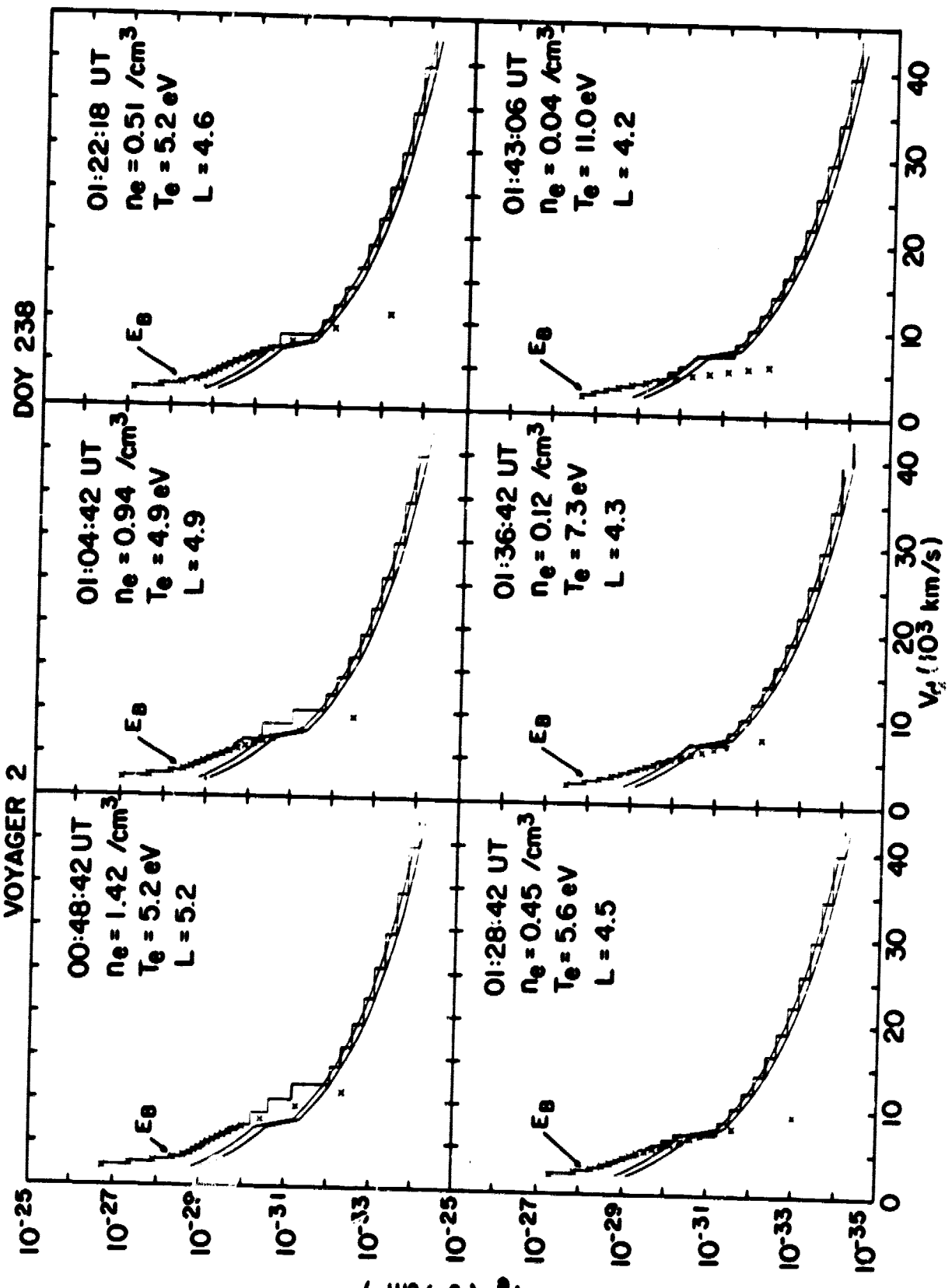

Figure 5

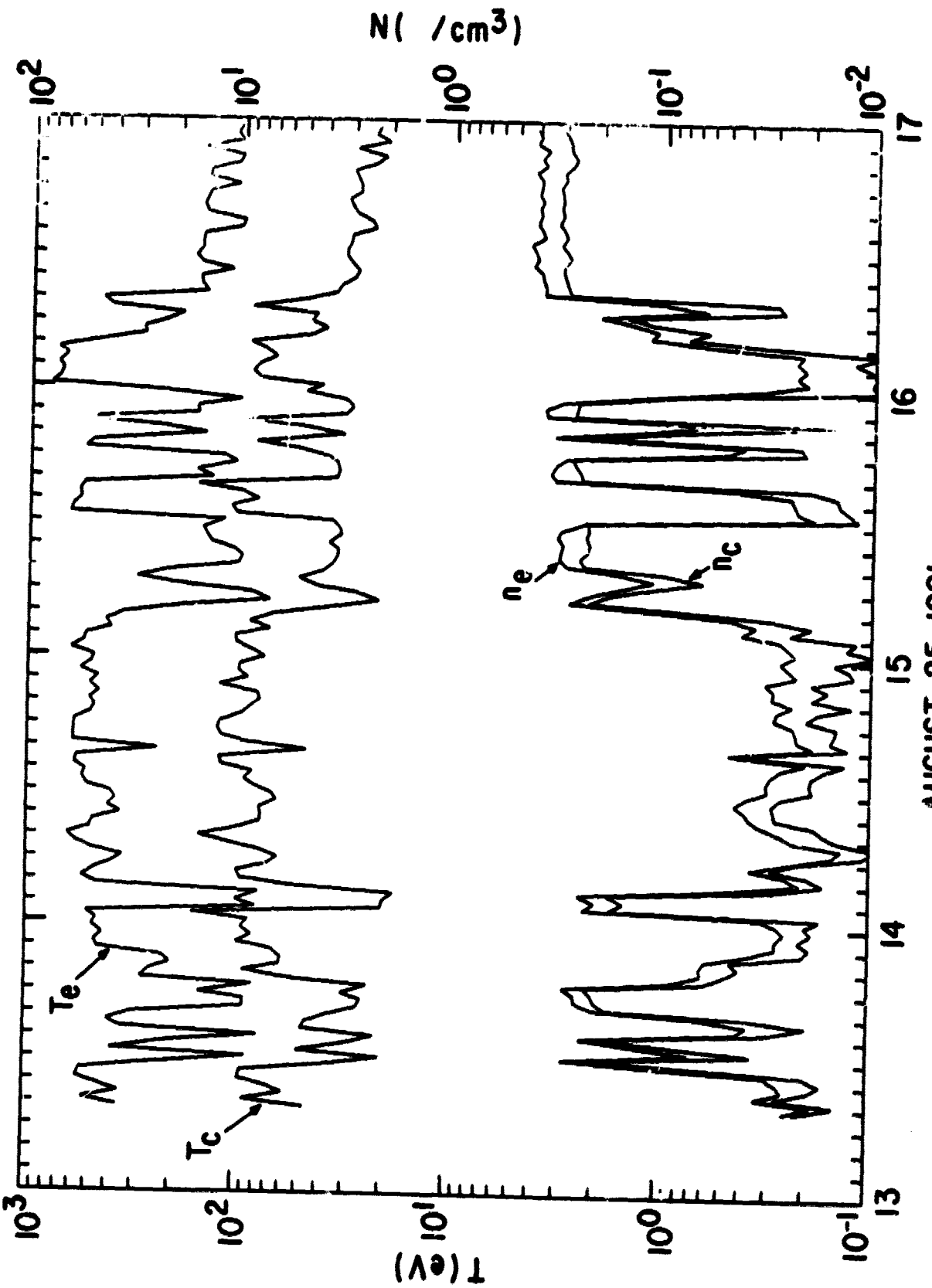

Figure 6

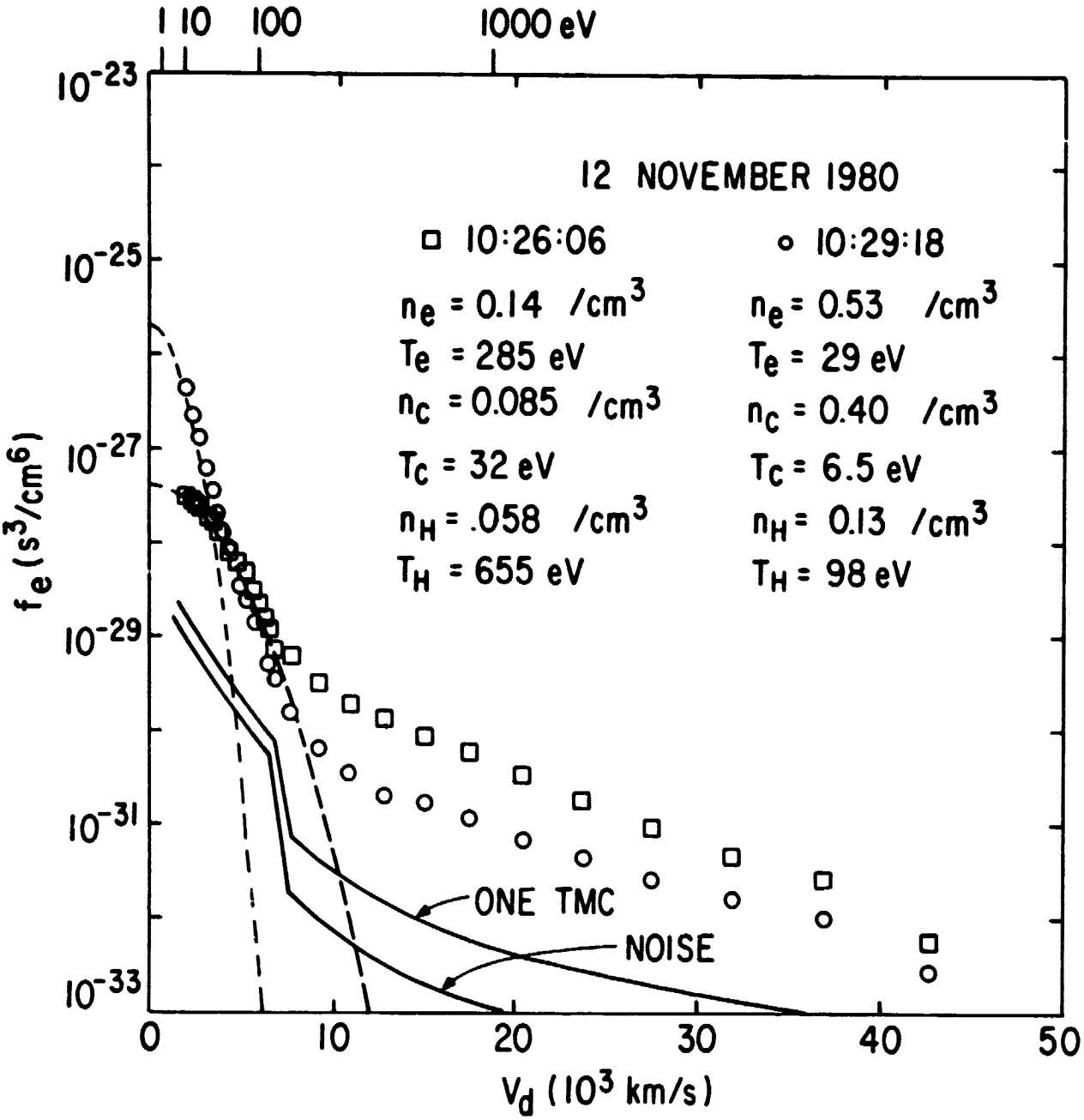

Figure 7

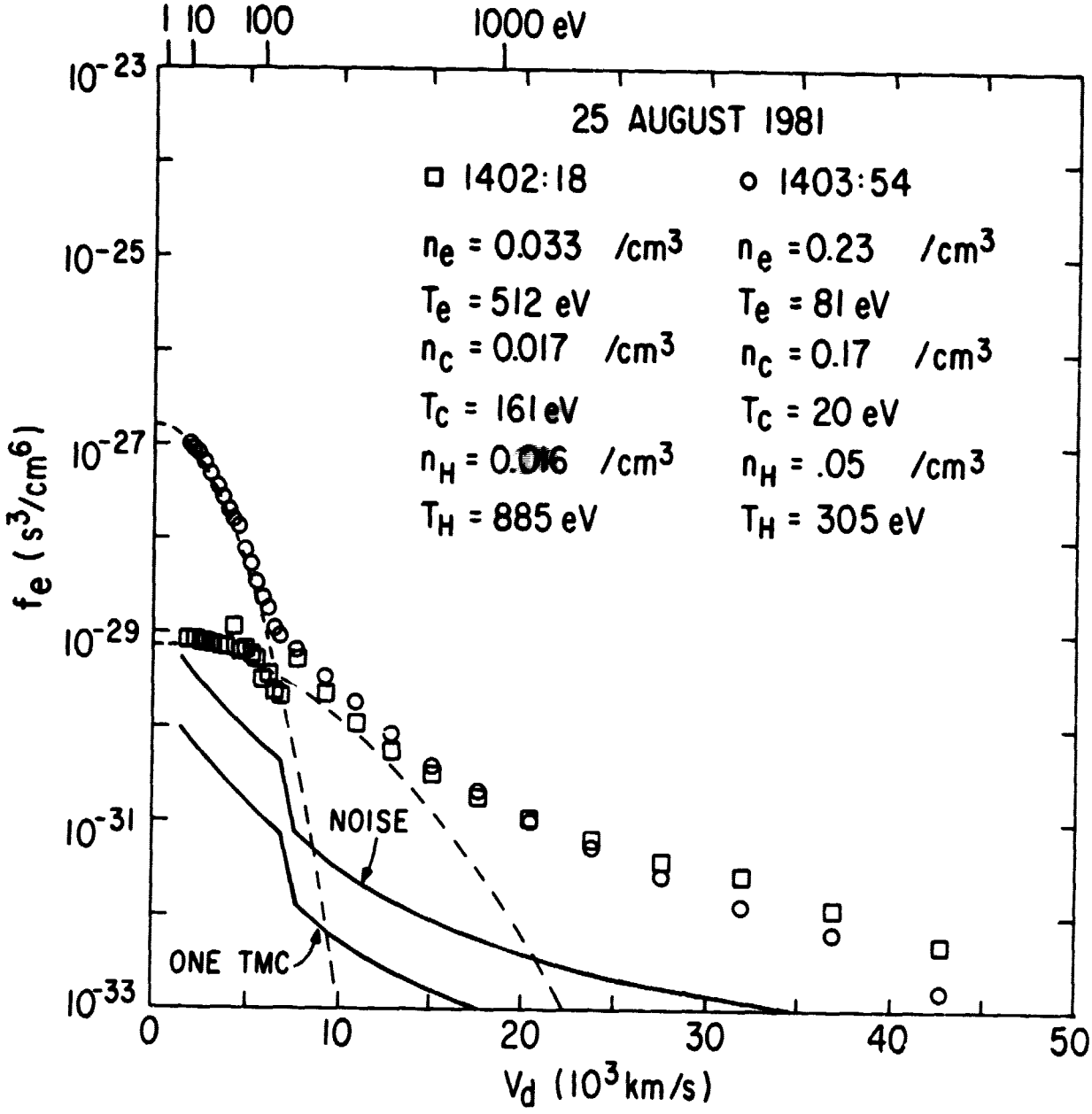

Figure 8

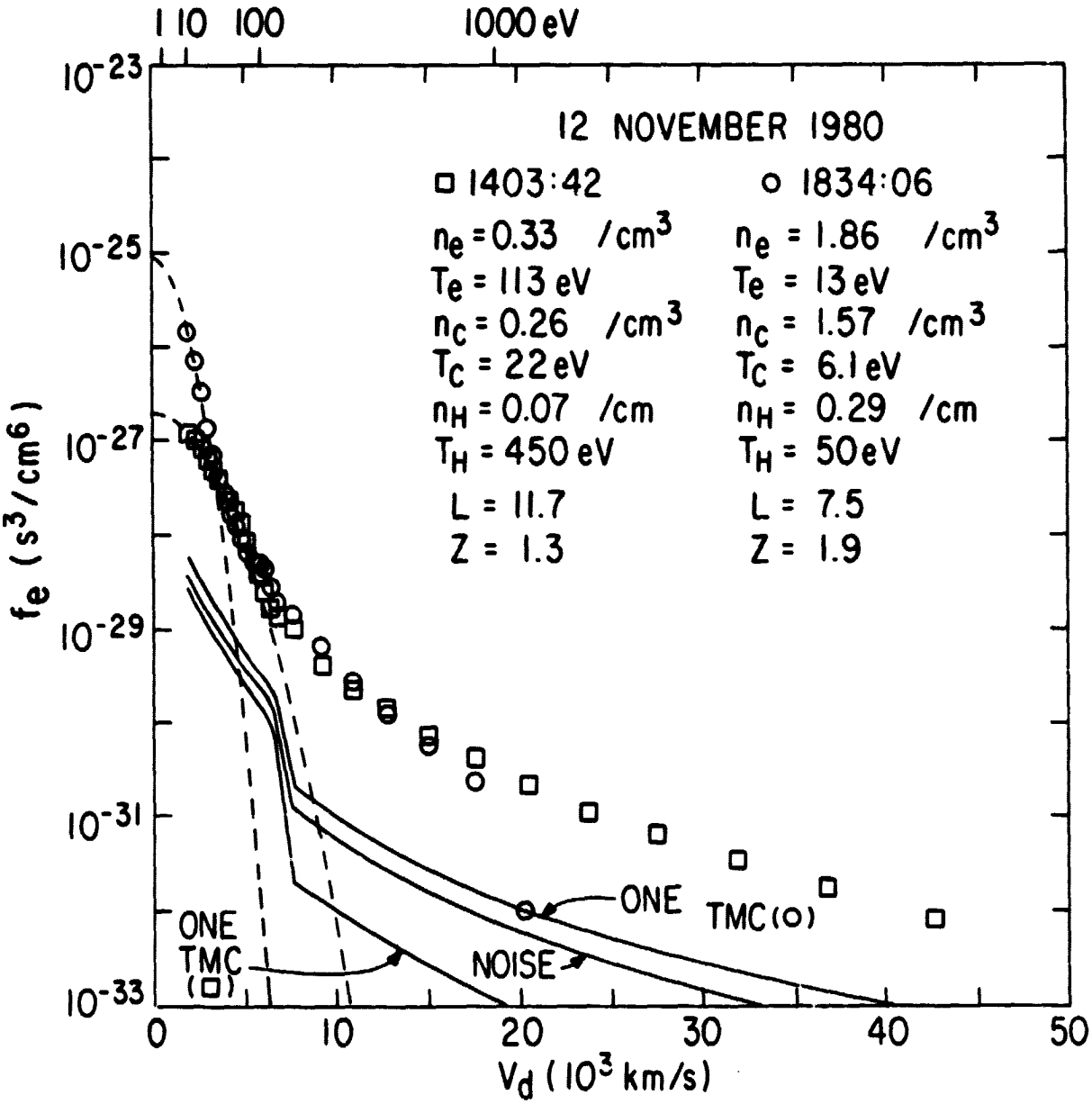

Figure 9

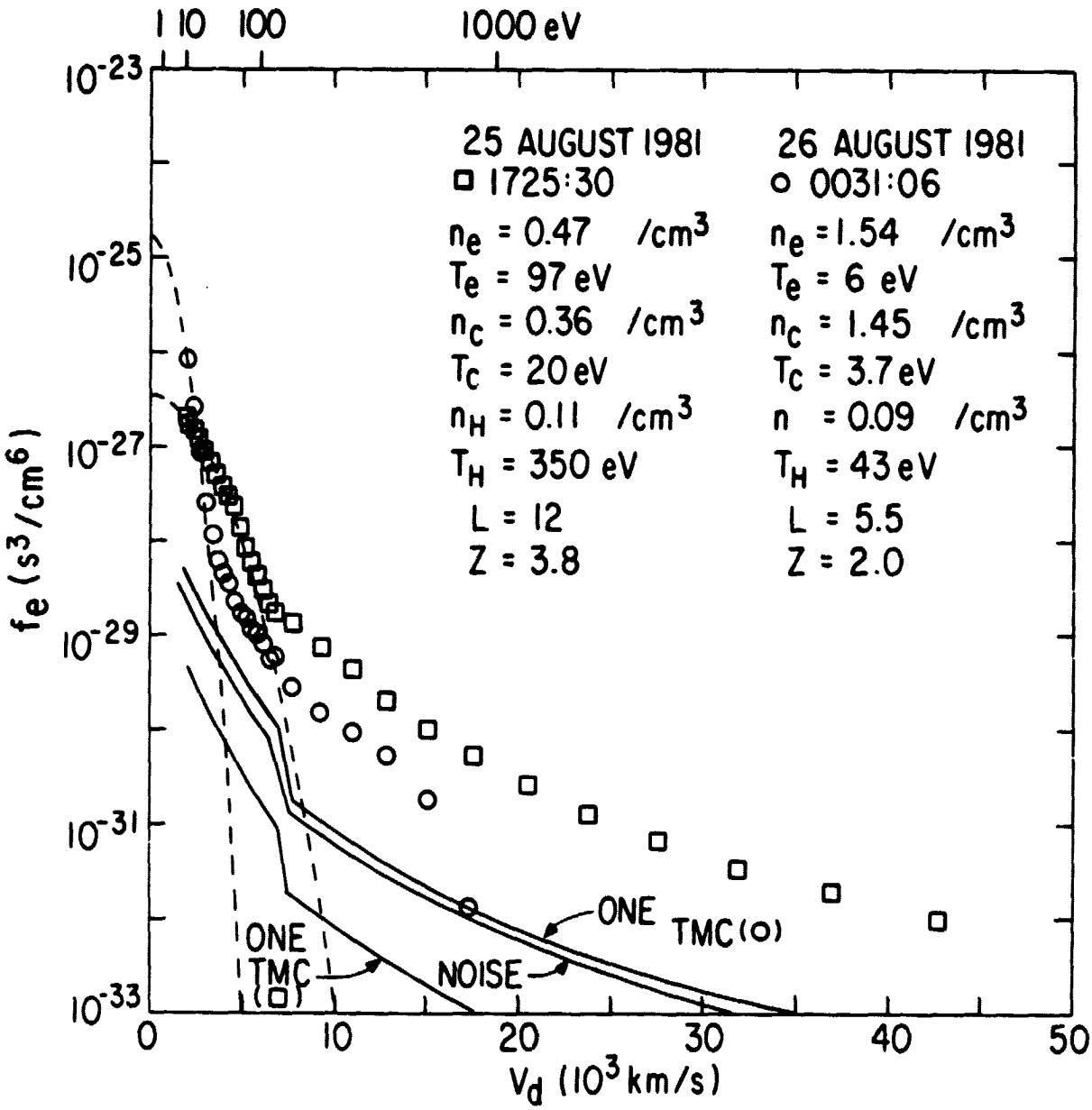

Figure 10

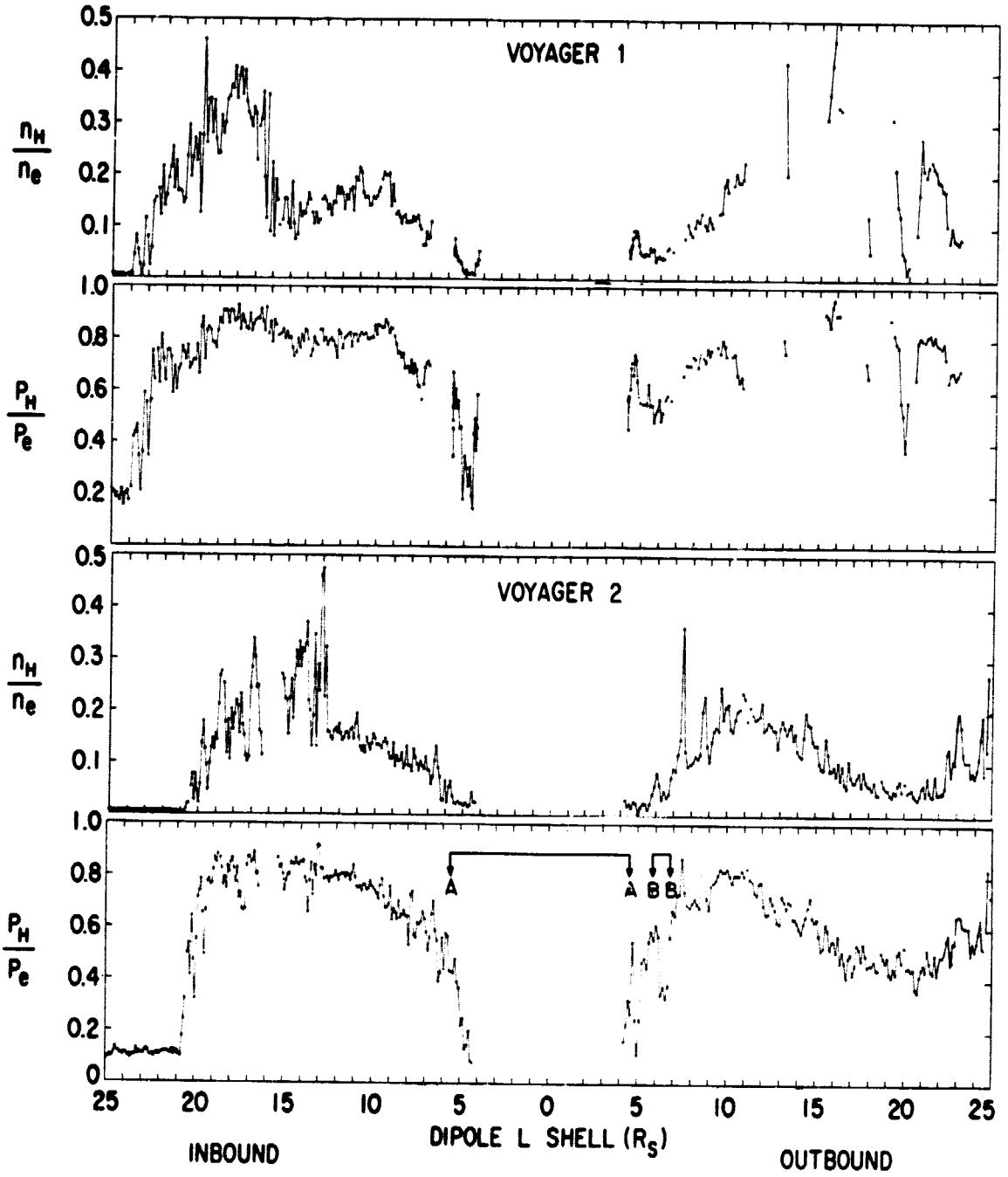

Figure 11

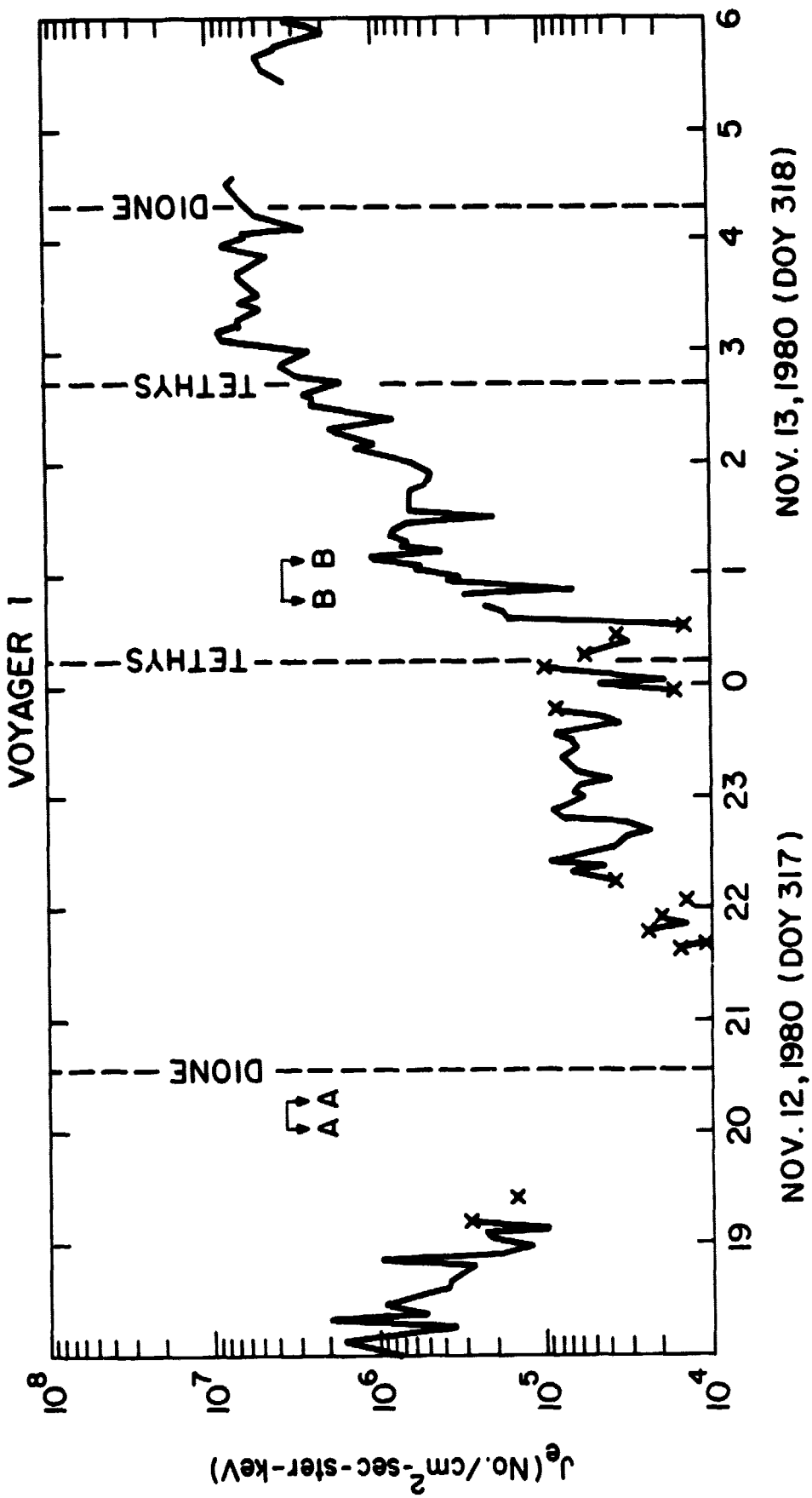

Figure 12

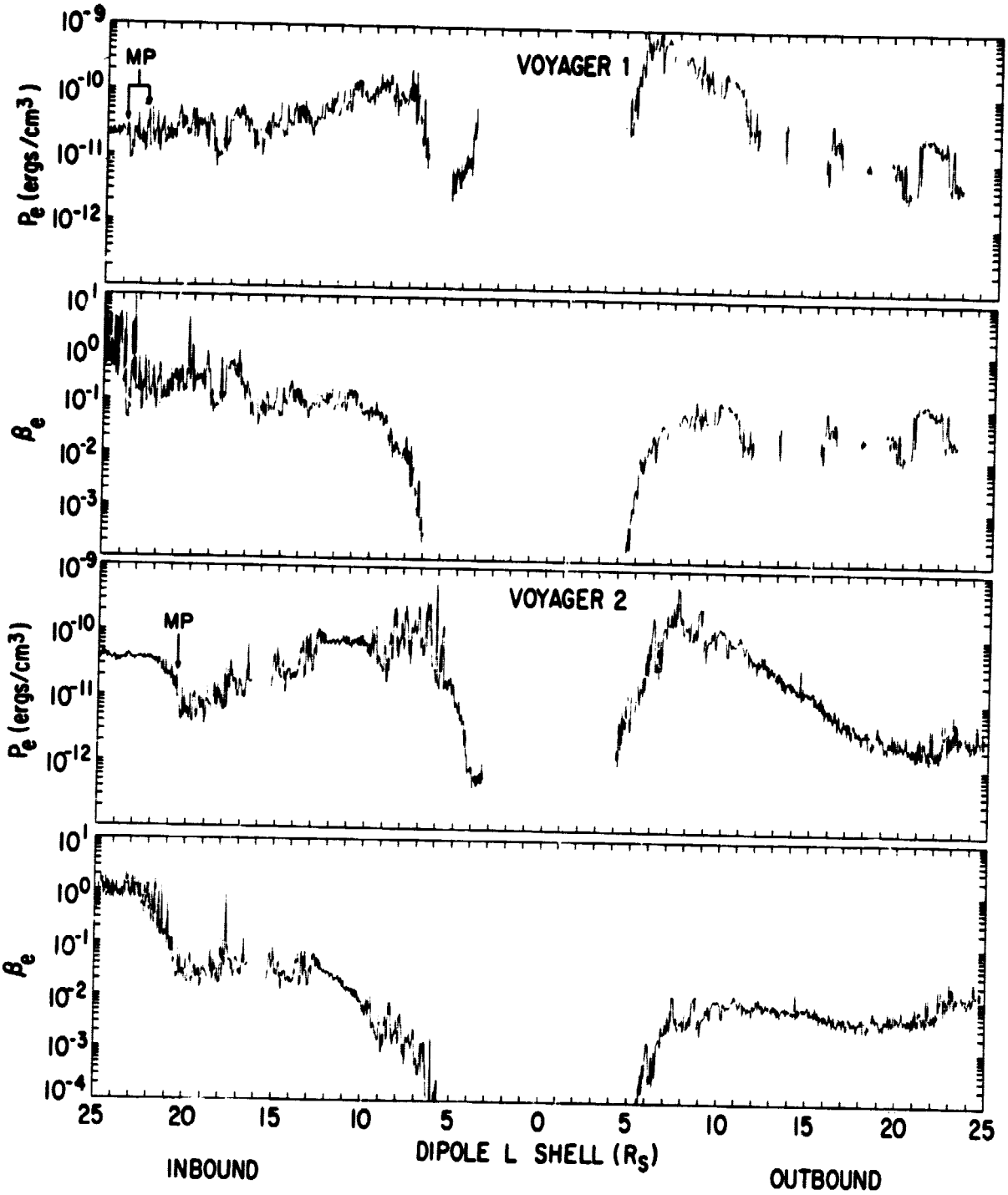

Figure 13

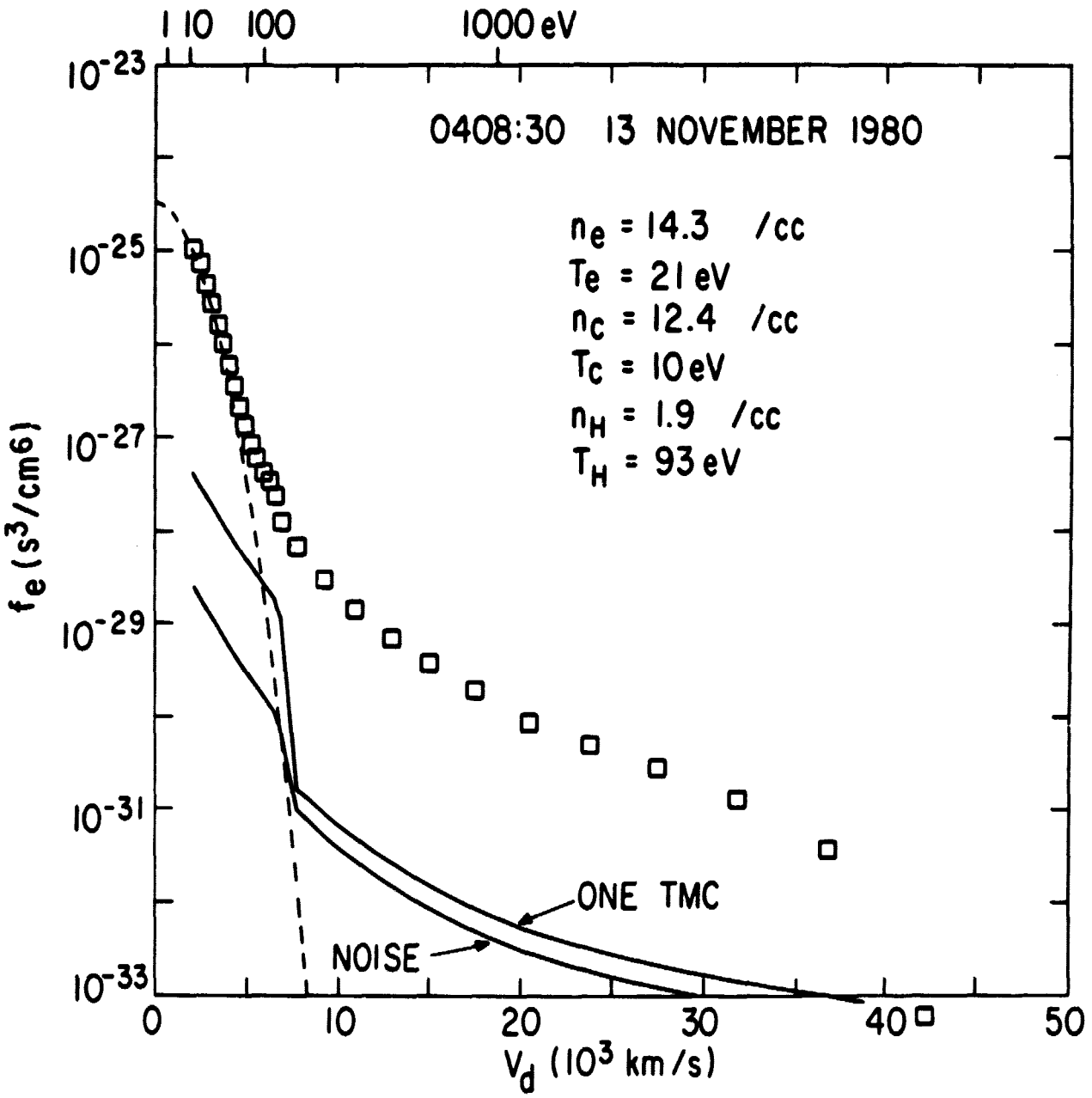

Figure 14

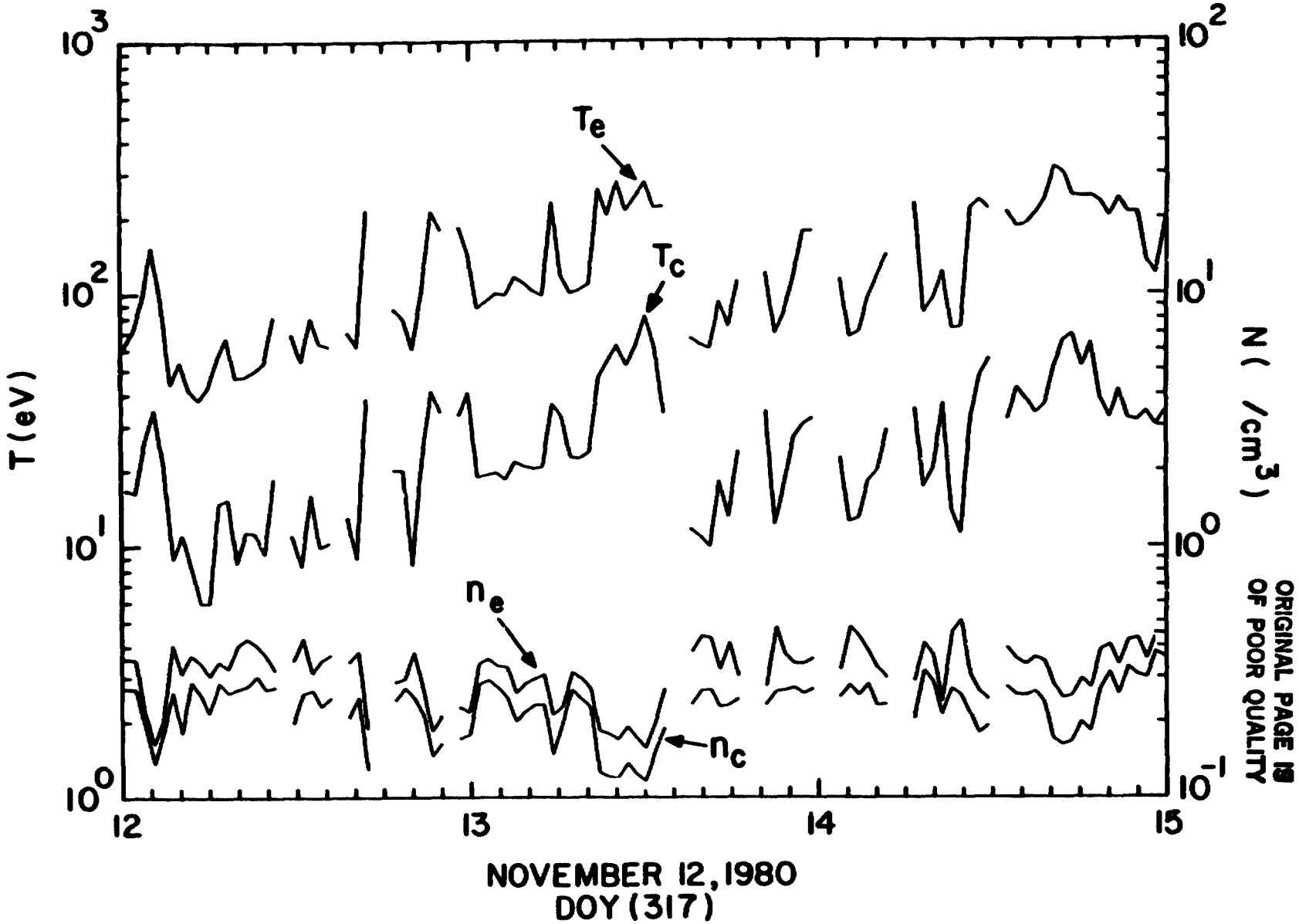
10^3
10^2
10^1
10^0
T(eV)
T_e
T_c
n_e
n_c
10^2
10^1
10^0
10^{-1}
N(/cm^3)
12
13
14
15
NOVEMBER 12, 1980
DOY (317)
ORIGINAL PAGE IS
OF POOR QUALITY

Figure 15

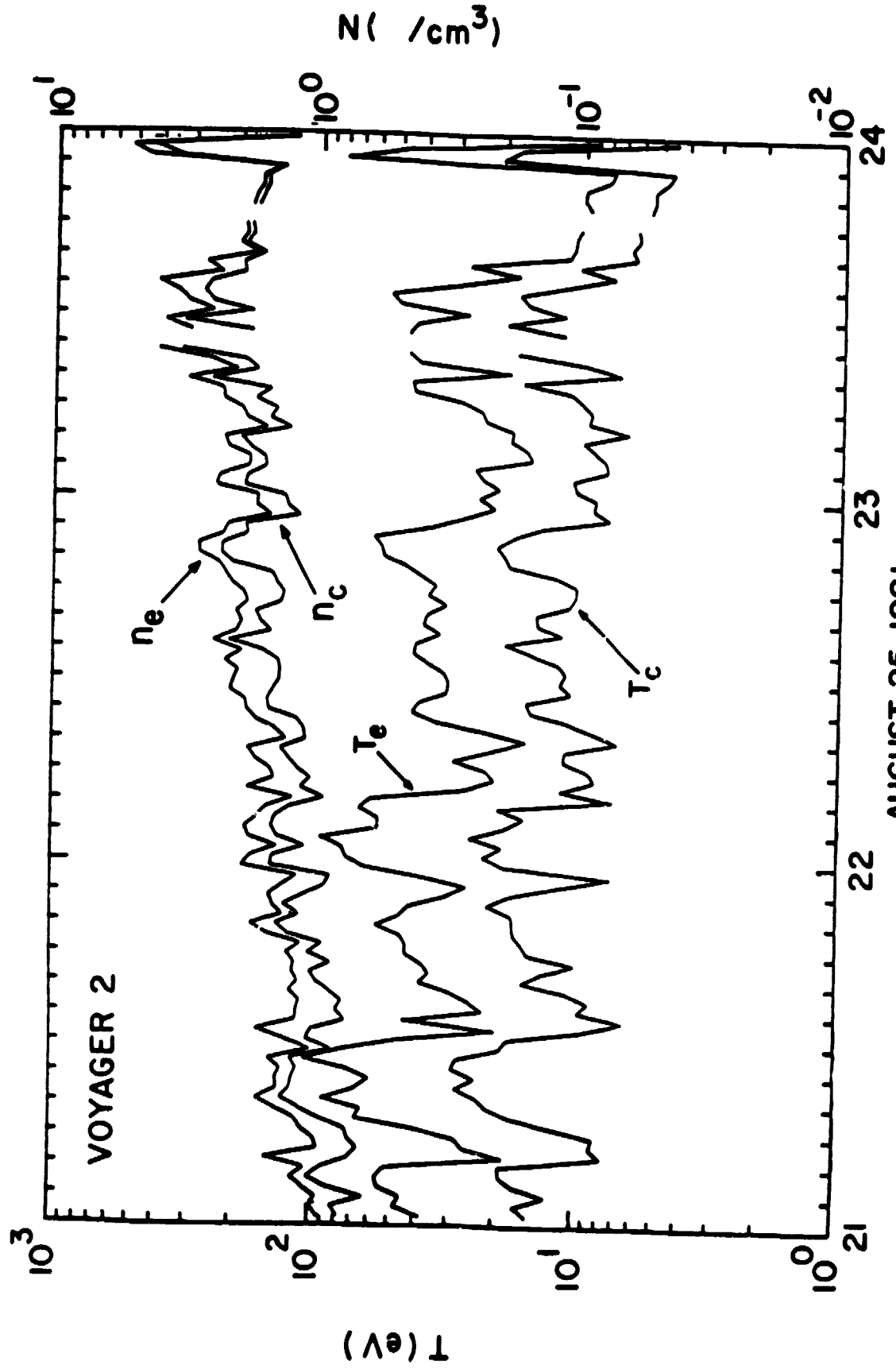

Figure 16